N76-32127

Final Report
on

AN INVESTIGATION OF DRAG-REDUCTION ON BOX-SHAPED GROUND VEHICLES

July 1976

KU-FRL #180

NASA Dryden Flight Research Center

Grant NSG 4004

Mr. Edwin Saltzman, Technical Officer

by
Vincent U. Muirhead
Principal Investigator
The University of Kansas

TABLE OF CONTENTS

LIST OF SYMBOLS

A cross-section area in in^2

E_o output voltage of a strain gauge bridge

I section moment of inertia in in^4

J section polar moment in inertia in in^4

K_g gauge factor of a strain gauge, i e , unit resistance change per unit strain

M bending moment in in-lb

Q torque in in-lb

R resistance in ohms

T thrust load in lb

V bridge excitation voltage

ε strain in microstrains, i e , micro-inches per inch

ε_B bending load induced strain

ε_Q torque load induced strain

ε_T thrust load induced strain

σ stress in psi

μ Poisson's Ratio

1 Introduction

This project, initiated in September 1971, has as its objective the determination of propeller design parameters which yield minimum propeller noise, given constraints on propeller performance

The study addresses both the theoretical and the experimental aspects of the problem Theoretical efforts have been directed at applying variational techniques to the noise equations Experimental efforts have been concerned with measurement of the propeller performance and noise of a Lockheed YO-3A aircraft

The following sections presents a report of the current state of this study

2 Theoretical Studies

The objective of the theoretical aspect of the program is to determine the optimum blade loading to minimize noise level, given the thrust, diameter, rotational speed and forward velocity. Both an aerodynamic model and an acoustic model for the propeller are required for this analysis

2.1 Aerodynamic Model

The aerodynamic model at present consists of a vortex system utilizing a lifting line and a helical vortex sheet for each blade The bladewise circulation distribution $\Gamma(y)$ is the sought for quantity in the noise minimization problem

A computer program has been written for the aerodynamic model based, essentially, on the analysis of Moriya (Ref. 2 1). The program, as it now stands assumes constant bladewise section aerodynamic characteristics. Modification to allow variable section aerodynamics is a relatively easy task and is now in progress The results of the aerodynamic analysis express the propeller performance in terms of the Fourier coefficients for the circulation distribution $\Gamma(y)$ A draft of this analysis is enclosed as Appendix A. Some further shakedown and check out of the program is required before it becomes fully operational

2.2 Acoustic Model

The acoustic model is a simplification of that represented by the Ffowcs-Williams-Hawkings equation (Ref 2.2, Eq 3-16) Presently only the force terms are retained, resulting in a model that is essentially Gutin's model with radially distributed line dipoles representing the blades Following successful treatment of this model, volume displacement effects will be included.

The sound intensity may be expressed in normalized form, as

$$I^* = \int_0^1 \int_0^1 F(r^*, r_1^*)\gamma(r^*)\gamma(r_1^*)dr^*dr_1^*$$

where γ is related to the circulation and F is a known function The constraint of constant thrust is expressed as

$$\int_0^1 \gamma(r^*)(1-r^*)dr^* = 1$$

Applying variational analysis to these equations provides a necessary condition for I^* to be a minimum

$$\int_0^1 F(r^*,r_1^*)\gamma(r_1^*)dr_1^* = -\frac{b}{2} r^*(1-r^*)$$

where b is a Lagrange multiplier.

Initial attempts at numerical inversion of this integral equation utilized both a Legendre Polynomial expansion and a Chebyschev polynomial expansion for $\gamma(r^*)$, coupled with a Gaussian integration procedure, reducing the integral equation to a matrix equation

$$AL = C$$

where L represents the unknown values of γ at selected points on the blade Numerical inversion of this matrix equation was not successful In all cases tried, the coefficient matrix A was ill-conditioned

The current approach involves a Fourier transform of the integral equation, implying the assumption that the noise is periodic in the blade frequency, with a Doppler shift This is consistent with the acoustic far-field assumption

Some success is indicated with this approach, however convergence is exceedingly slow and, as a consequence, required computer time is large

Appendix B contains some details of the earlier analysis for a simplified case in which only the thrust component of blade lift was included.

Appendix C contains some details of the current analysis utilizing Fourier Transforms.

2 3 References

2 1 Moriya, T., "Selected Scientific and Technical Papers," University of Tokyo, Tokyo, 1959

2.2 Goldstein, M E , "Aeroacoustics," National Aeronautics and Space Administration, Washington, D C , 1974

3. Experimental Activities

All experimental efforts have been directed toward in-flight measurements of propeller torque and thrust and fly-by sound levels, utilizing a YO-3A aircraft

3 1 Aircraft Preparation

Since the YO-3A aircraft was received in disassembled, worn and damaged condition, a good deal of time and effort has been spent rendering it airworthy. Much of this effort was expended in obtaining maintenance and operating manuals, shop drawings, etc. The cooperation in these endeavors of Mr Harold Schuetz, USAAVSCOM, St Louis, and Mr. David Schnebly, Lockheed, Sunnyvale, is very gratefully acknowledged

Major repairs have included a top overhaul on the engine, repair of a fractured vertical fin-fuselage attachment fitting, repair of aileron and wing tip damage, replacement of elevator attachment pins, manufacture of special jigs for checking drive shaft/prop shaft alignment and belt tension, modification of the forward instrument panel, installation of VHF radio, removal and repair of the muffler system, and other items Photographs of the aircraft and the propeller drive systems are shown in Figures 3 1 and 3 2

3.2 Measurement of Propeller Performance

3 2.1 Introduction

An essential element in the development of a low-noise propeller is the accurate measurement of its propulsive performance This means that the thrust available, the thrust power available, and the shaft power required must be measured, preferably in flight For the subject studies, a

Lockheed YO-3A aircraft is available for use as a test platform A significant part of the program has been devoted to instrumenting this aircraft for the in-flight measurement of thrust and power

Two approaches to these measurements were considered in this study

a) Airflow Measurement

By pressure surveys of the flow field behind the propeller, determinations of the thrust and torque acting on the propeller are possible (Ref 3.1) However, this method requires correction for the interference effects of the fuselage The accuracy of this method was judged insufficient for the purposes of this project

b) Direct Thrust and Torque Measurements

The YO-3A's propeller is mounted on a cantilevered propeller shaft (Figures 3 2 and 3 3) This shaft is driven through a speed reduction drive system employing pulleys and belts Because of this drive system, the engine is isolated from the shaft and load cell measurements on the engine mounts would not yield propeller thrust data Such measurements could produce approximate torque measurements if pulley, belt and propeller shaft bearing losses could be determined

As shown in Figure 3.3, approximately 9-inches of the propeller shaft is easily accessible The strains induced in this shaft are direct measures of the thrust and torque transmitted to the propeller Thus, direct instrumentation of the propeller shaft (say, with strain gauges) can, in principle, yield the desired information This approach was selected

There is one major difficulty involved in this approach, i e , the thrust related strains are much smaller than the torque related strains and are very small in an absolute sense No mechanical modifications to the shaft (e g weakening the shaft in tension) were attempted because of airworthiness questions involved Instead, it was decided to attempt to measure the shaft strains directly

3 2 2 Propeller Shaft Loads

The YO-3A aircraft is powered by a Continental IO-360A engine rated at 210 hp at 2800 rpm It drives a 3-bladed, constant-speed propeller through a sheave and belt system that provides a 3 33 1 speed reduction ratio. The blade pitch is controlled by a Woodward governor that supplies pressurized engine oil to the propeller through the hollow propeller shaft

Based on data given in Reference 3 2 and assuming no drive system losses, it is estimated that a maximum of 186 hp is available at the propeller shaft to drive the propeller This, together with a propeller shaft speed of 841 rpm, yields a maximum torque to be transmitted by the shaft of 13,944 in -lbs.

Again based on data from Reference 3 2, it appears that the thrust required in level flight, at sea-level, will be in the range from 250 to 400 lbs. Although performance data are not available for the propeller, the assumption of an efficiency of 50% at the sea-level stalling speed of 61 knots yields an estimated maximum thrust available of about 500 lbs. The thrust load instrumentation has been designed on the basis of a maximum thrust load of 500 lbs, but can measure thrust loads up to 1000 lbs

Besides the torque and thrust loads, the shaft is subject to loads from three other sources

a) Bending Due to Propeller Weight

Bending stresses due to the weight of the propeller are estimated to be due to a 1500 in -lb moment acting about the location of the instrumentation on the shaft

b) Internal Oil Pressure

The internal oil pressure produces an axial tension stress due to the action against the hub piston. It also produces a hoop stress (tension) that, through Poisson's ratio, induces a compressive axial stress The net effect is a small axial tension stress. This net stress is about 28 psi for an oil pressure of 100 psi; this is equivalent to an additional thrust load of about 53 lbs

c) Centrifugal Force

At a shaft speed of 841 rpm, the outer surfaces of the shaft has an acceleration of about 24 g's The resulting axial stress is negligible compared to the other shaft stresses

Table I summarizes the stresses and strains in the propeller shaft due to thrust, torque, and bending Both the centrifugal stresses and the net oil pressure stresses as calculated were negligible, however, their effects will be evaluated during calibration of the instrumentation The ratios of the maximum strains taken from Table I are

$$\varepsilon_{T_{max}} : \varepsilon_{M_{max}} \quad \varepsilon_{Q_{max}} \cdot 1 \quad 66 . 424$$

These ratios show the crux of the instrumentation problem, i e., the very low thrust strains in the presence of much larger bending and torque strains

3 2 3 Strain Transducer Arrangements

The sensor choice was dictated by the need to distinguish between the combined loads present, as well as the need to measure them reliably and accurately The sensor must also function over the range of environmental conditions met in aircraft flight. Strain gauges were chosen as the sensors

Most strain gauge work is done in the 50-500 microstrain range, within this range it is possible to measure changes of 1 or 2 microstrains However, the thrust strains on the shaft are 8.85 microstrains full scale, see Table I. This low strain level poses problems in the thrust measurement The torque and bending strain levels are high enough to present no difficulties in reliable measurement by foil strain gauges

Figure 3.4 outlines the decision process followed in choosing the method of measurement and selection of sensors Two main avenues of approach were made for the thrust measurement

1) Intensification of the low level thrust strains by mechanical means, using foil strain gauges as sensors.

2) Direct shaft strain measurement of thrust strains Foil strain gauge and semi-conductor strain gauge evaluations were made and compared The semi-conductor gauges are 75 times as sensitive as foil gauges but have a high inherent temperature effect on sensitivity as compared to foil gauges

Wheatstone bridges, with an active strain gauge in each arm were chosen If all four arms experience equal temperature changes, and if all four gauges are perfectly matched then temperature effects are automatically cancelled. Figures 3 5 and 3.6 illustrate the directions of the strains produced by the thrust, bending, and torque loads and the bridge arrangements used for measuring them. Each of the strains can be measured independently of the other two and, in each case, the bridge output exceeds the output of a single active gauge

When the shaft is subjected to thrust, bending and torque, the induced strains act along certain directions, as shown in Figure 3.5 Thrust and bending loads produce tensile and compressive strains in the axial direction Due to the Poisson effect, axial tensile and compressive strains generate compressive and tensile lateral strains. The shear strains induced by torque cause tensile/compressive strains on mutually perpendicular axes inclined at 45° to the shaft axis, the sum of the components of torque strains in the axial and lateral directions are zero The sums of the thrust and bending strain components, in the torque strain directions, are not zero but their effects on the torque bridges will cancel

Figure 3 6 shows the three arrangements of strain gauges used to measure thrust, bending and torque on the shaft, taking advantage of the directional properties just discussed Referring to this figure, we have

Thrust. $E_o = \frac{Kg}{4} [2(1+\mu)\varepsilon_T]$ V

Torque $E_o = \frac{Kg}{4} [4\varepsilon_Q]$ V

Bending $E_o = \frac{Kg}{4} [4\varepsilon_B]$ V

Ignoring second order effects, non-linearities and cross-sensitivities of the gauges, and assuming the gauges are perfectly matched and aligned in the required directions, each of these bridge arrangements reacts only to one type of loading and is insensitive to the other two loads

3.2 4 Mechanical Intensification of Thrust Strain

Larger thrust strains can be obtained by adding a load path parallel to the propellant shaft and incorporating in this added path a short, weak link

Such an arrangement is shown in Figure 3.7. The propeller shaft (1) carries most of the thrust load The parallel load path (made up of the support link (2) and the weak link (3)) carries only a small part of the thrust load, the amount is determined by the relative strengths of the weak link and the propeller shaft However, both load paths stretch equally under the load Because most of the stretching of the parallel path occurs in the short weak link, its strain is much greater than that of the shaft, i e , $\varepsilon_3 >> \varepsilon_1$

An analysis of this strain intensifier arrangement yields the following intensification ratio

$$\frac{\varepsilon_3}{\varepsilon_{1_o}} = \frac{\ell_1}{\ell_3}\left[\frac{1}{1 + \left(\frac{\ell_1}{\ell_3}\right)\left(\frac{A_3E_3}{A_1E_1}\right) + \left(\frac{\ell_2}{\ell_3}\right)\left(\frac{A_3E_3}{A_2E_2}\right)}\right]$$

where

ε = strain, micro-inches per inch

ℓ = length

A = cross-sectional area

E = modulus of elasticity

The subscripts 1, 2, and 3 refer to the components as shown in Figure 3.7 and ε_{1_o} is the shaft strain in the absence of the intensifier If the tensile strength of the weak link is made much less than those of the support link and the propeller shaft such that

$$\left(\frac{\ell_1}{\ell_3}\right)\left(\frac{A_3E_3}{A_1E_1}\right) << 1$$

and

$$\left(\frac{\ell_2}{\ell_3}\right)\left(\frac{A_3E_3}{A_2E_2}\right) << 1$$

then the intensification ratio is approximately

$$\frac{\varepsilon_3}{\varepsilon_{1_o}} \approx \frac{\ell_1}{\ell_3}$$

The system used to study the performance of the strain intensifier is shown in Figure 3.8. The system consisted of two weak link assemblies, 180° apart, mounted on a full-scale model of the exposed portion of the propeller shaft. The links were fabricated of aluminum and were each instrumented with 4-arm strain gauge bridges. Using the smallest gauges available, a link length of 0.2 inches was achieved, yielding a length ratio, ℓ_1/ℓ_3, of 40. The thickness and width of the links were 0.010 and 0.400 inches, respectively. The tensile strength ratios were

$$\frac{A_3E_3}{A_1E_1} \cong 0.003$$

$$\frac{A_3E_3}{A_2E_2} \cong 0.001$$

The test assembly was installed in a lathe (Figure 3.9) and could be loaded simultaneously in torque, bending, and thrust. Loadings up to 40% of full-scale were used. Typical results of the thrust calibration are shown in Figure 3.10, and the overall thrust and the torque interactions with thrust results are summarized in Table II. It is evident that the torque interaction is very large. Over the full-scale range of loads to be met in flight, the weak link system would have an output, due to torque interaction, of 860% and 212% of the full-scale thrust output. (The interaction results of the two links are different due to different arrangements of the gauges on each link. This was done to check the effect of gauge arrangement on the torque interaction.) Because of the large torque interaction effects and because the links required very close machining tolerances and were found to be very difficult to install and adjust satisfactorily, the mechanical strain intensifier was rejected as a practical solution to the thrust measurement problem.

A second attempt at mechanical intensification was made using a deflection sensor manufactured by DSC, Inc In this device, a small cantilevered arm is instrumented with semi-conductor strain gauges to measure the bending strains produced by deflection of the end of the arm The deflection sensitivity appeared very attractive for the present application, i.e , about 6μV/V/μ-inch compared to a shaft strain of 8.85 microstrain for the 500 lb thrust load

The sensor's arm has a flexure near its end to reduce the effects of bending moments other than those due to linear deflections It was hoped that this feature also would help reduce the torque and bending interactions in the thrust measurement Tests of several different installation arrangements showed, however, that the interactions were much worse with this sensor. Because of this, it was rejected as a possible thrust sensor

3.2 5 Direct Shaft Strain Measurements

With the abandonment of mechanical strain intensification, a study of the practical problems of direct thrust strain measurement was undertaken. For comparison purposes, both foil and semi-conductor strain gauges were used In the case of the foil gauges (which have low strain sensitivity but good temperature characteristics), both 120 ohm and 350 ohm gauges were used The latter gauges were used to take advantage of the higher excitation voltages possible. The semi-conductor gauges (which have high strain sensitivity but poor temperature characteristics) were 1000 ohm gauges with gauge factors of about 155

The gauges were mounted on the model propeller shaft and were installed in the lathe (see Figure 3 9) and loaded in combined thrust and torque. The torque sensor was made up of 350-ohm foil gauges fabricated as special purpose torque rosettes Typical results are presented in Figures 3.11 and 3.12 The results are summarized in Table II For comparison purposes, the expected sensitivity of the foil bridge was

$$\frac{E_o}{VT} = .023 \text{ micro-volts/volt/lb thrust}$$

and the expected sensitivity of the semi-conductor bridge was

$$\frac{E_o}{VT} = 1\ 78 \text{ micro-volts/volt/lb thrust}$$

From the results of Table II it was concluded that the foil gauges are adequate for the torque measurement However, the higher sensitivity of the semi-conductor gauges was found necessary for reliable measurement of the small thrust strains Since the aircraft will produce a noisy environment for the instrumentation system and since the sensor signals will be transmitted from the rotating shaft through slip rings, it is important that the sensor outputs be as large as possible to insure a high signal-to-noise ratio

The selection of semi-conductor strain gauges for the thrust measurement was made in spite of their poor temperature sensitivity characteristics. The resistance of these gauges increases while the gauge factor decreases as the gauge temperature increases These temperature effects can be reduced by placing a suitable resistance (called a span resistor) in series with the bridge This resistor has a negligible resistance change with temperature As the bridge resistance increases (reducing the circuit current), the voltage drop across the span resistor decreases and voltage drop across the bridge increases This increase in bridge (excitation) voltage tends to compensate for the decrease in bridge sensitivity The value of the span resistance can be used to control the temperature range over which compensation is achieved.

The effectiveness of temperature compensation was studied by installing an electric resistance heater inside the model shaft and measuring bridge output as a function of bridge temperature (which was monitored by thermistors mounted near the gauges). Some typical results from this study are presented in Figure 3 13. These results show that the uncompensated bridge has a temperature sensitivity of 12.3 μV/V/°F That is (for a bridge initially balanced at 78 °F) at a bridge temperature of 104 °F, the temperature induced output would be about 40% of the full-scale thrust output However with a 915 ohm span resistor, this bridge, at 104°F, will have a temperature induced output of only 5% of the full-scale thrust output. In flight, the propeller shaft temperature will change due to changes in both ambient temperature and oil temperature inside the shaft. Thus, temperature compensation of the semi-conductor bridges will be mandatory In addition, surface temperatures will be measured so that corrections in bridge output can be made.

The results presented in Figure 3 14 and Table II, show that there is a large torque interaction bridge output. This interaction possibly can be explained by one of the following arguments Theoretically there should be no torque strain components in the axial and lateral directions, which are the directions in which the thrust gauges are mounted This is true provided that the thrust gauges are exactly aligned on the shaft axes, and that the shaft is isotropic and homogenous In the present case, the ratio of the maximum thrust and torque strains is 1 42 4 Thus, small misalignments of the thrust gauges from the shaft's axial and lateral directions would cause a pickup of torque strain components that might be sizeable compared to the small thrust strains. The term misalignment here is meant to include both the deviation of the gauges from the axial and lateral directions caused in gauge mounting, as well as the deviation of the shaft axis from its theoretical direction.

For the full-scale loads, the thrust and torque interactions per degree of gauge misalignment have been calculated to be·

> A maximum torque strain interaction of 96 8% of the maximum thrust strain would occur for each degree of misalignment of the thrust gauges
>
> A maximum thrust strain interaction of 2.23% of the maximum torque strain would occur for each degree of misalignment of the torque gauges

Another possible source of this interaction could be the cross-sensitivity of the gauges This is normally a very small effect, but in the present case it may be significant because of the 1 42 4 ratio of maximum thrust and torque strains.

For both the foil and semi-conductor thrust bridges, whose results are presented in Table II, the torque induced output was of a sign opposite to the thrust output. (The sense of the applied torque was the same as that which would occur in the aircraft) When the sense of the torque was reversed, the sign of the torque induced strains also changed Both the foil and semi-conductor gauges were mounted on a shaft which had buckled slightly in an earlier test Before the gauges were installed, the shaft was remachined, but the buckling could have caused a curved shaft axis

Another test shaft was made and a new set of semi-conductor gauges were mounted on it When this shaft was tested under the same conditions as the older shaft, the torque interaction in the thrust bridge output was still present but its maximum value had been reduced to 44 3%. Also, torques applied in the same sense as that in the aircraft, produced torque induced strains of the same sign as the thrust induced strains This result is opposite to that observed with the older shaft This result tends to support misalignment as a cause of the interaction It is very difficult to exactly predict the misalignment effect because four individual gauges are involved However, for both the old and the new shafts, the torque interaction was calibratable and repeatable

A bending interaction in the thrust output was also observed. This interaction was much smaller than the torque interaction The bending interaction can also be caused by misalignment, as well as by small differences in the sensitivities of the gauges making up the thrust bridges For the new shaft, the maximum interaction was only 7 05%. This bending interaction also was found to be calibratable and repeatable

3.2 6 Instrumentation Development and In-Flight Systems Description

3 2.6.1 Introduction and Background

A block diagram of the thrust/torque measuring system is presented in Figure 3 15. The elements of this system can be grouped into three subsystems, (1) strain measurement components mounted on the propeller shaft, (2) components located in the cockpit, and (3) auxiliary components. By way of background, a short discussion of the development of the strain measurement system is presented first

Because of the very low thrust-induced strain levels, a high gain system with a high signal-to-noise ratio is required if the thrust measurement is to be successful Initially an AC system, with a 1000 Hz carrier frequency, was designed and built. This system exhibited sufficient sensitivity and was quite linear However, the zero-strain bridge output could not be nulled, even when the bridge was resistance balanced Furthermore, this zero load minimum bridge output level was sufficient to saturate the first amplification stage. Is is thought that the problem was due to phase unbalance between the semi-conductor bridge arms In view of this problem, the system was redesigned to use DC excitation throughout The DC system, which will be used for in-flight testing, has been built and is now being checked out on a full scale model of the propeller shaft. With the exception of the data recorder, all components of the instrumentation system receive power from a regulated $\pm$ 15 VDC power supply operating from the 400 Hz aircraft electrical system

3.2 6.2 Components on the Propeller Shaft

The thrust, torque, and bending transducers (4-arm strain gauge bridges) are mounted directly on the propeller shaft The associated electronics are mounted on a printed circuit board that is attached to the front face of the slip-ring assembly (see Figure 3 16 and Section 3 2 6 3 below) Bridge excitation is by a regulated, IC 5 VDC power supply that is part of the shaft instrumentation package and operates from the 15 VDC source This additional regulation was selected to provide a stable source for the strain transducer circuits

The bridge outputs are processed by IC differential amplifiers feeding into operational amplifiers (See Figure 3.17). The amplifier combinations are adjusted to give overall gains of 1000 The amplifiers are mounted in high thermal resistance packages and have active internal temperature controls giving very tight temperature control This arrangement provides highly stable gain and low temperature drift over a range of ambient temperatures from -55°C to + 125°C.

3 2 6.3 Slip Ring Assembly

A sectional view of the slip ring assembly is shown in Figure 3.18 and a photograph of the components, before final assembly, is presented in Figure 3 19. The brush/ring material combination was selected on the basis of information given in Reference 3 3 and after some preliminary laboratory checks The objective was a low resistance contact and very low slip ring noise The materials selected were hard brass rings and silver-graphite (50% silver by weight) brushes Two brushes and two internal leads are provided for each ring to further improve the contact characteristics.

In order to avoid the complications of a split slip ring assembly, the inside diameter of the assembly is 5 inches, large enough to slip over the flange at the forward end of the propeller shaft (see Figure 3 2) A split spacer is clamped to the shaft, to bring the diameter up to 5 inches Two aircraft quality bearings separate the inner (rotating) and outer (fixed) assemblies. The outer assembly is thus carried by the shaft and is not rigidly attached to the aircraft frame. A soft rotational restraint will be used, minimizing vibration effects.

3 2.6 4 Cockpit Components

An amplifier control box and a data recorder are located in the observer's (forward) cockpit The control box contains active filters, having 3db roll-off at about 65 Hz, and output amplifiers for use in adjusting the overall gain of the system (See Figure 3 20) It will also contain auxiliary components discussed in Section 3 2.6 5 below

The data recorder is a Gulton Industries, 8-channel, strip chart recorder provided by the University's Aviation Research Laboratory (ARL) where it has been used for in-flight testing. It is powered by a 400 Hz to 60 Hz inverter, also supplied by ARL

A bundle of shielded co-axial cables will connect the slip-ring brushes to the amplifier control box

3.2 6 5 Auxiliary Instrumentation

In order to correct the semi-conductor bridge output for temperature effects, thermistors will be mounted on the shaft surface close to the strain gauges They will be connected to the cockpit control box through the slip rings and the cable Associated electronics will be contained on the printed circuit board on the shaft and in the control box Their output will also be recorded on the 8-channel recorder

The apparent thrust load will contain a contribution due to the oil pressure in the shaft This pressure will be monitored by a pressure transducer in the hydraulic line between the governor and the propeller shaft. Its associated electronics also will be in the control box with output recorded on the 8-channel recorder

Finally the control box will contain a single stage timer to provide a time reference for the recorder output

3.3 Fly-by Noise Measurements

Capability of fly-by noise measurements has been established Measuring equipment consists of a General Radio 1962-9601 microphone with associated pre-amps and power supply, feeding into a NAGRA IV-SJ tape recorder. Analysis of the results is accomplished by use of a General Radio 1564-A Sound and Vibration Analyzer The noise recording and analysis equipment is University supplied

Procedural checks of the noise measuring program have been satisfactorily completed.

Weather conditions with sufficiently low ambient noise level to allow detection of the very low noise level of the YO-3A aircraft have not prevailed at this writing This aspect of the program is ongoing and aircraft noise measurements will hopefully be achieved in the near future

3.4 References

3.1 Vogley, A. W., "Climb and High-Speed Tests of a Curtis No. 714-1C2-12 Four-Blade Propeller on the Republic P-47C Airplane", NACA ACR No. L4L07, 1944.

3.2 Condon, G. W., Rundgren, I. W., and Davis, W. B., "Army Preliminary Evaluation I, YO-3A Airplane, Final Report", US Army Aviation Systems Test Activity, August 1970.

3.3 Dutee, Phillips, and Kemp, "Operating Stresses in Aircraft Engine Crankshafts and Connecting Rods Part I, Slip Ring and Brush Combinations for Dynamic Strain Measurements", NACA MR E5C30.

3.5 Bibliography

3.1 Dean M , and Douglas R , "Semi-Conductor and Conventional Strain Gauges," Academic Press, New York and London

3 2 Murray W., and Stein P , "Strain Gauge Techniques," MIT Press

3.3 Perry C , and Lissner H , "The Strain Gauge Primer," McGraw Hill.

3 4 Stein P , "Measurement Engineering," Arizona State University Press

Figure 3.1 The YO-3A Aircraft with Cowl Removed

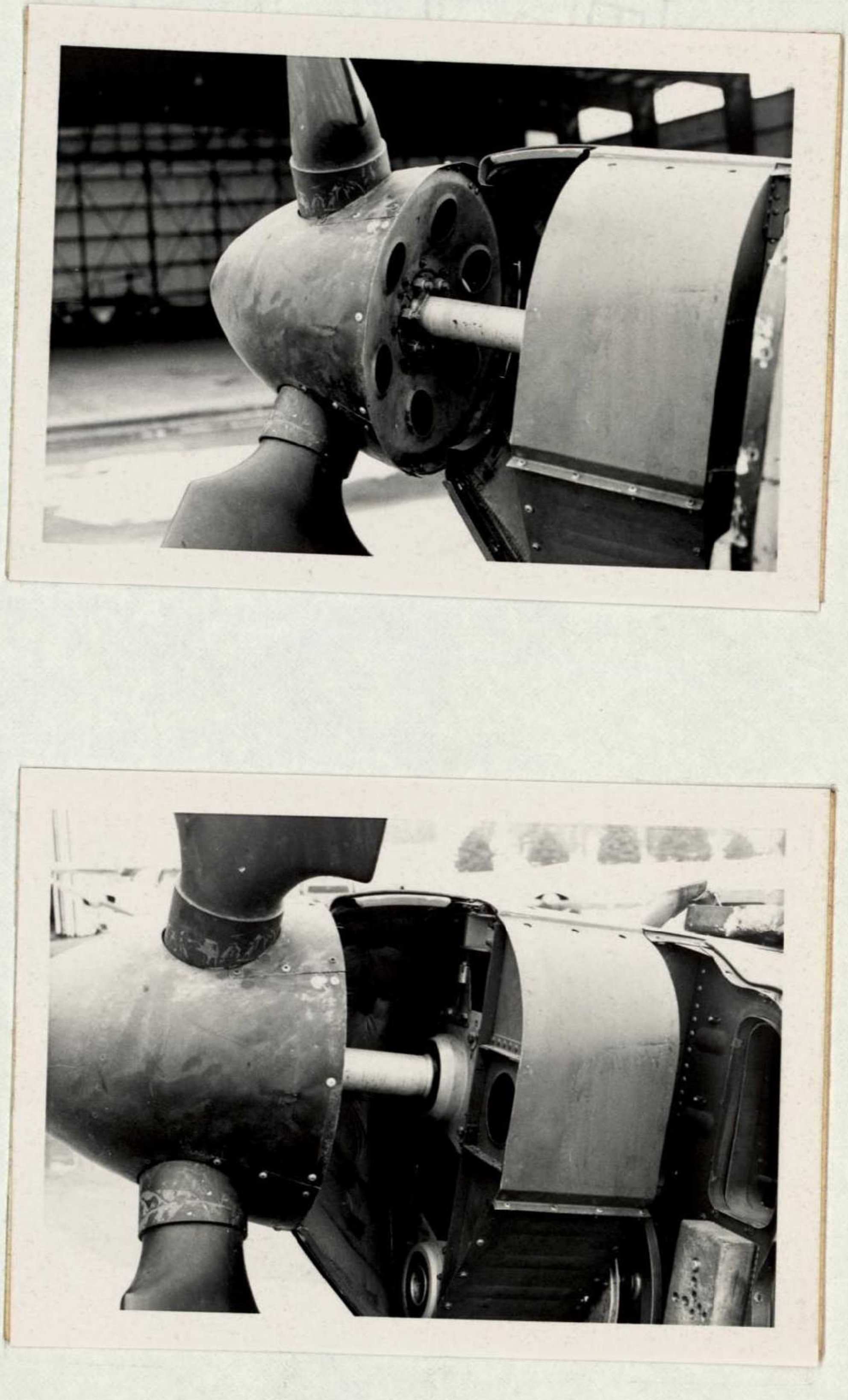

Figure 3.2 The YO-3A's Propeller Shaft and Hub

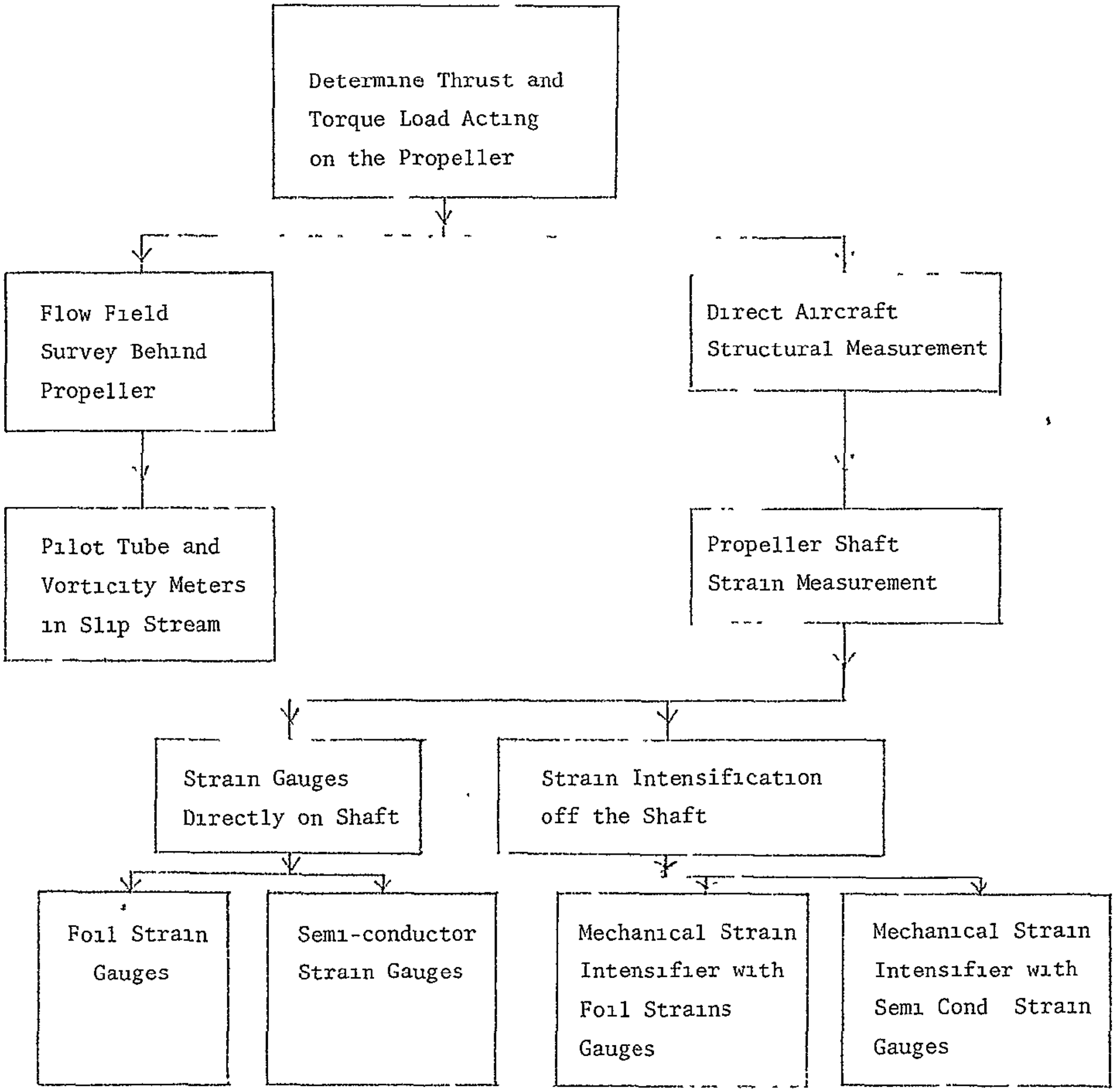

Figure 3.4 Approaches to the In-Flight Measurement of Propeller Performance

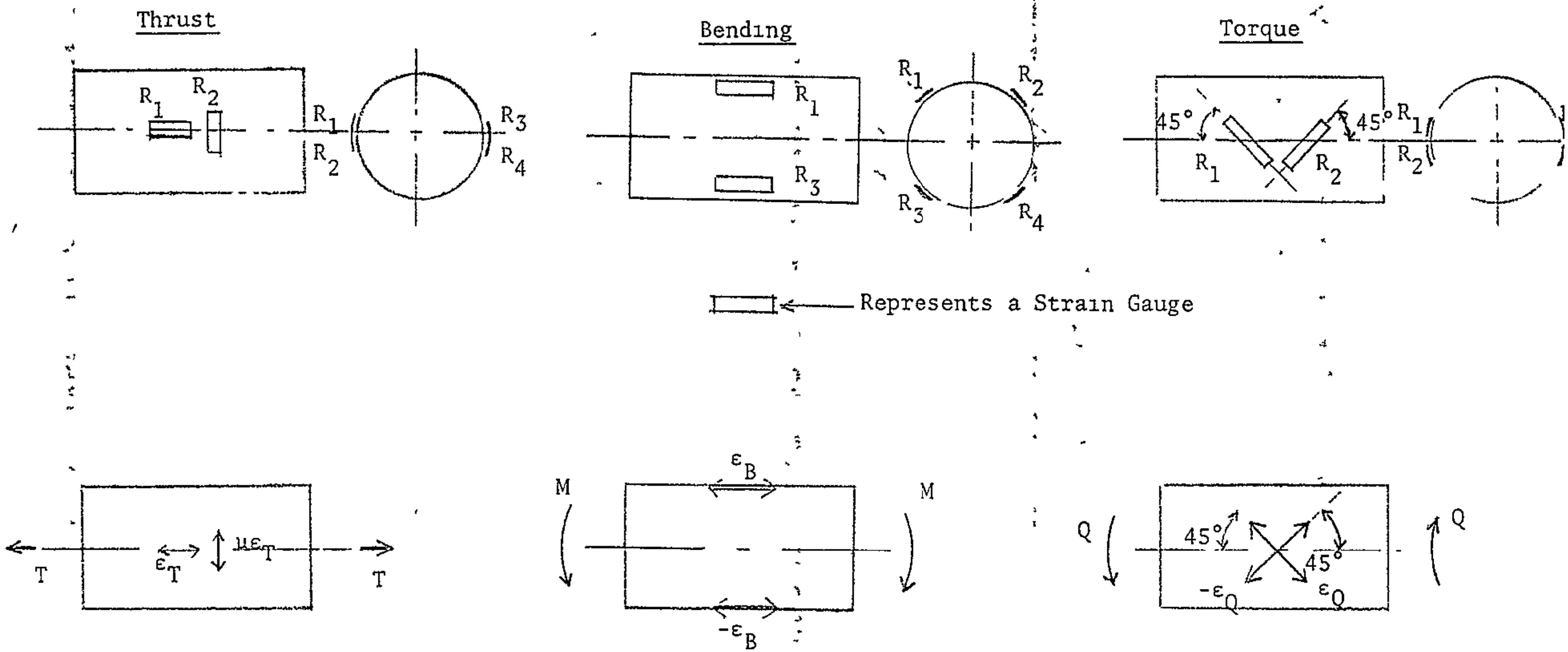

Figure 3.5 Propeller Shaft Strain Gauge Arrangements and Strain Directions

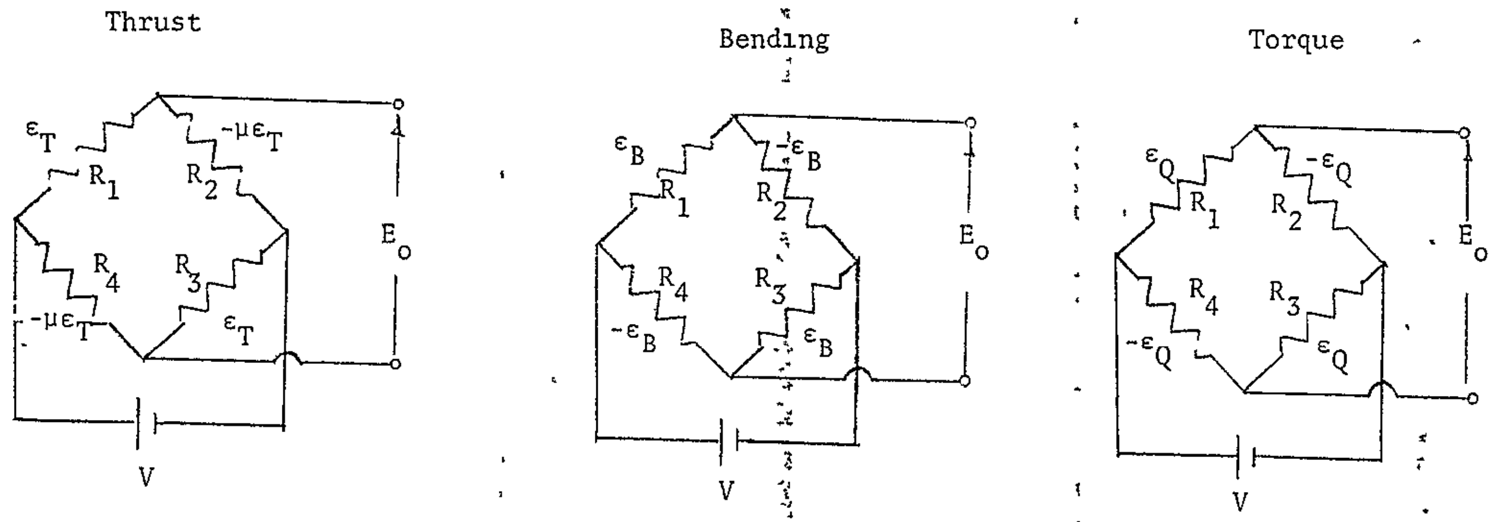

μ = Poisson's ratio of the shaft material

μ = 0 3 for steel

$$E_o = \frac{Kg}{4}\,[2(1+\mu)\varepsilon_T]V$$

$$E_o = \frac{Kg}{4}\,[4\varepsilon_B]V$$

$$E_o = \frac{Kg}{4}\,[4\varepsilon_Q]V$$

Figure 3.6 Thrust, Bending and Torque Strain Bridge Circuits

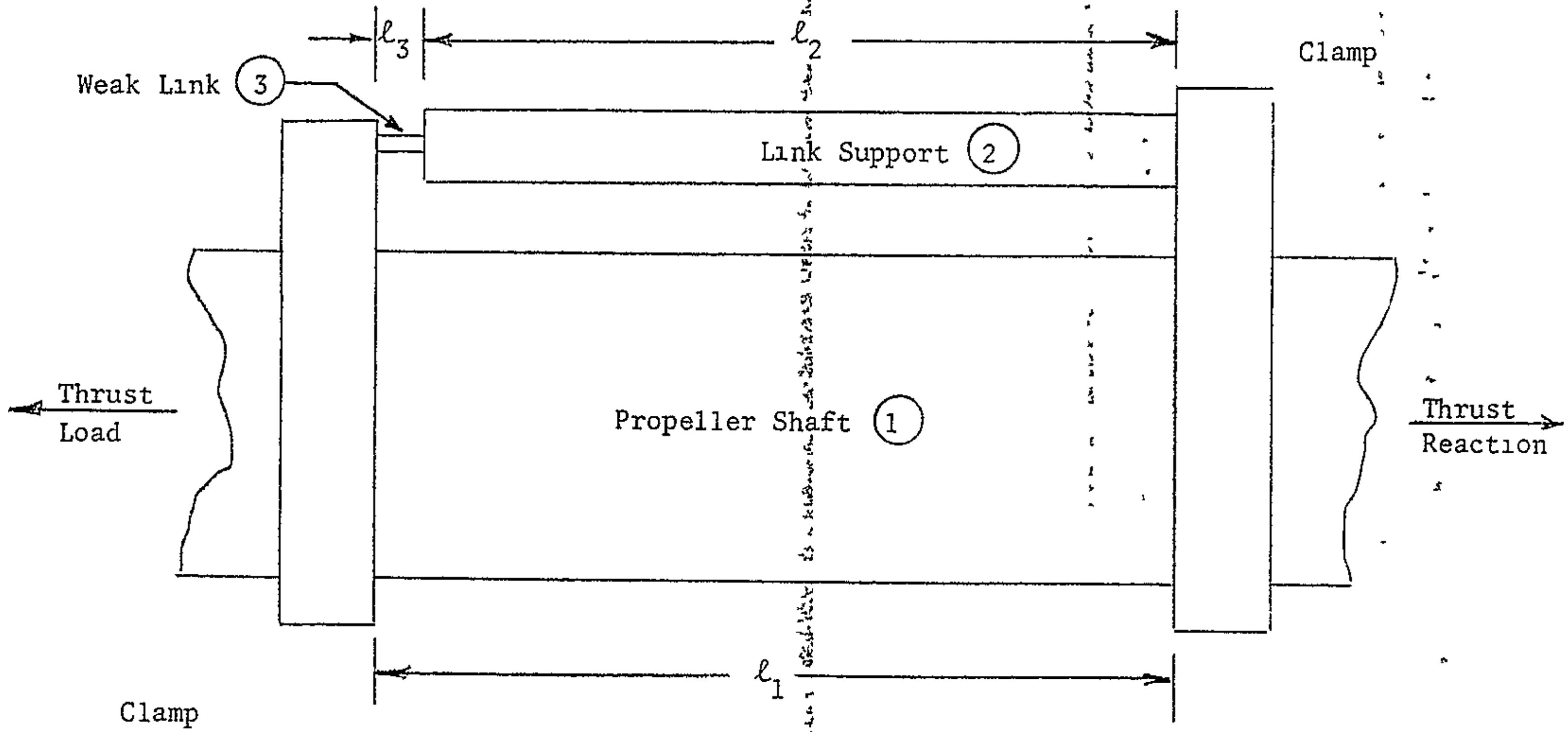

Figure 3.7 Schematic of Mechanical Strain Intensifier

Intensifier I

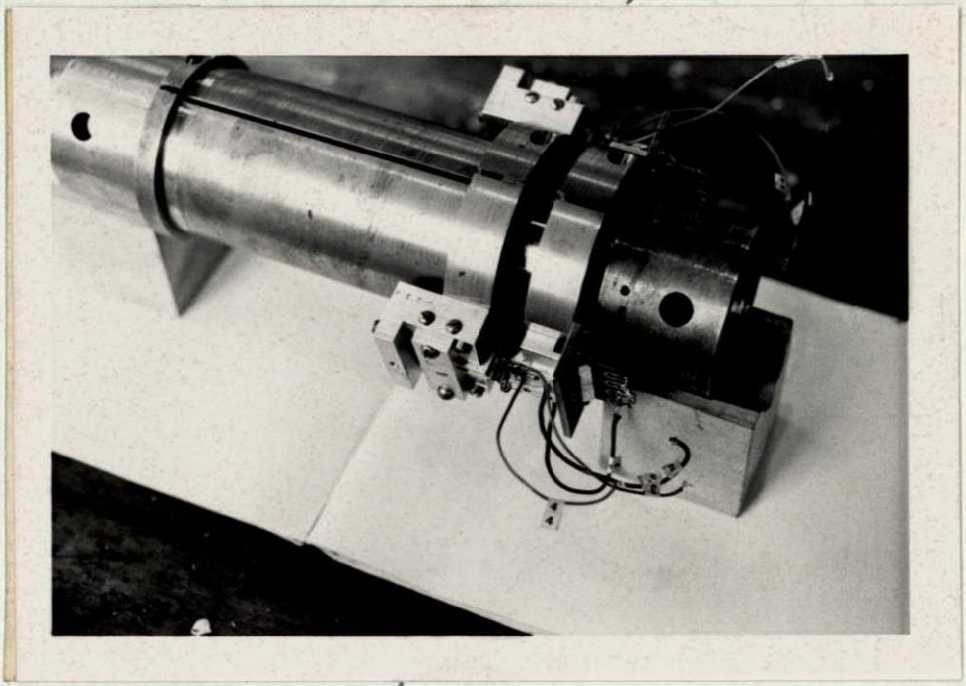

Intensifier II

Intensifier I

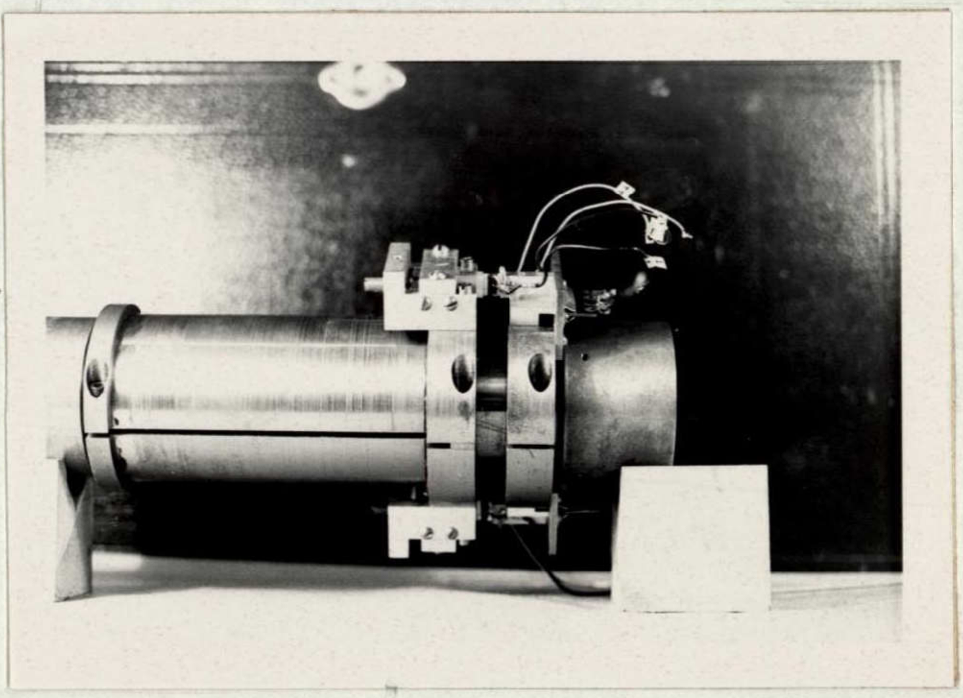

Figure 3.8 Mechanical Thrust Strain Intensifier, Mounted on Model Propeller Shaft

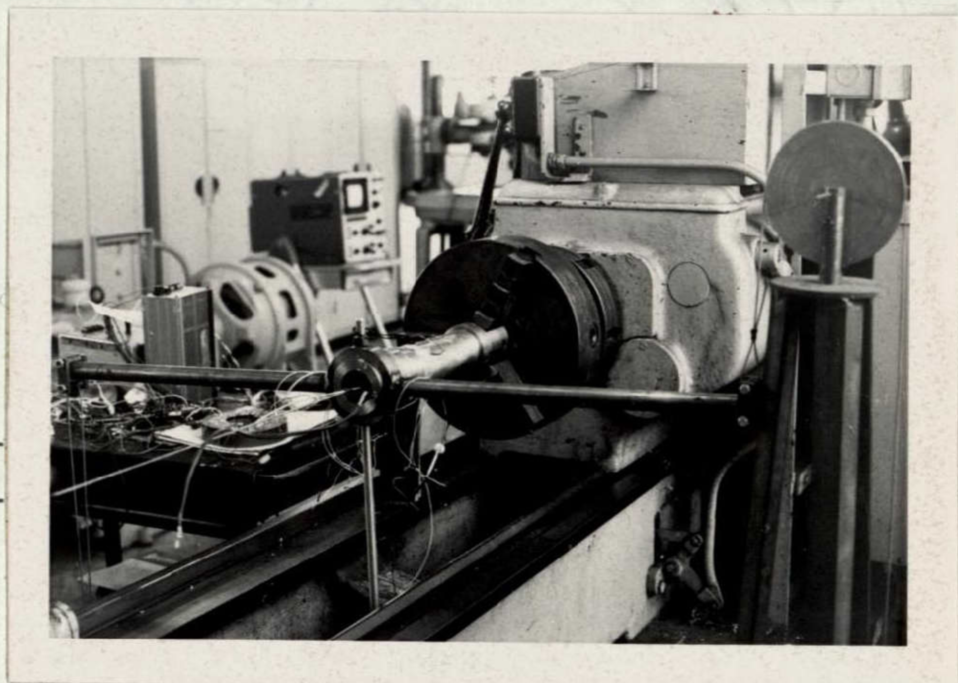

Figure 3.9 The Combined Loading Arrangement for the Model Shaft

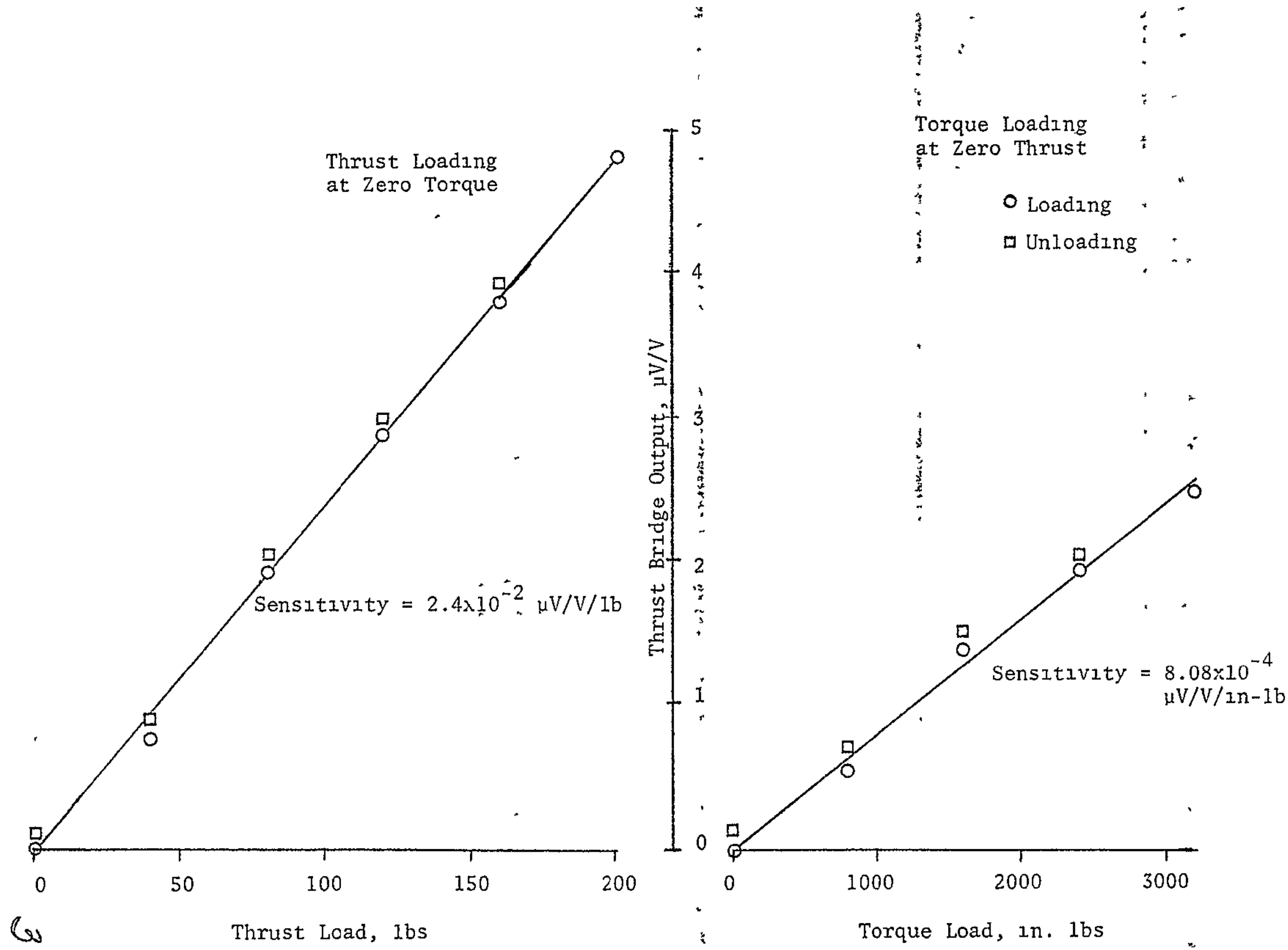

Figure 3 11 Foil Thrust Bridge Calibration

29

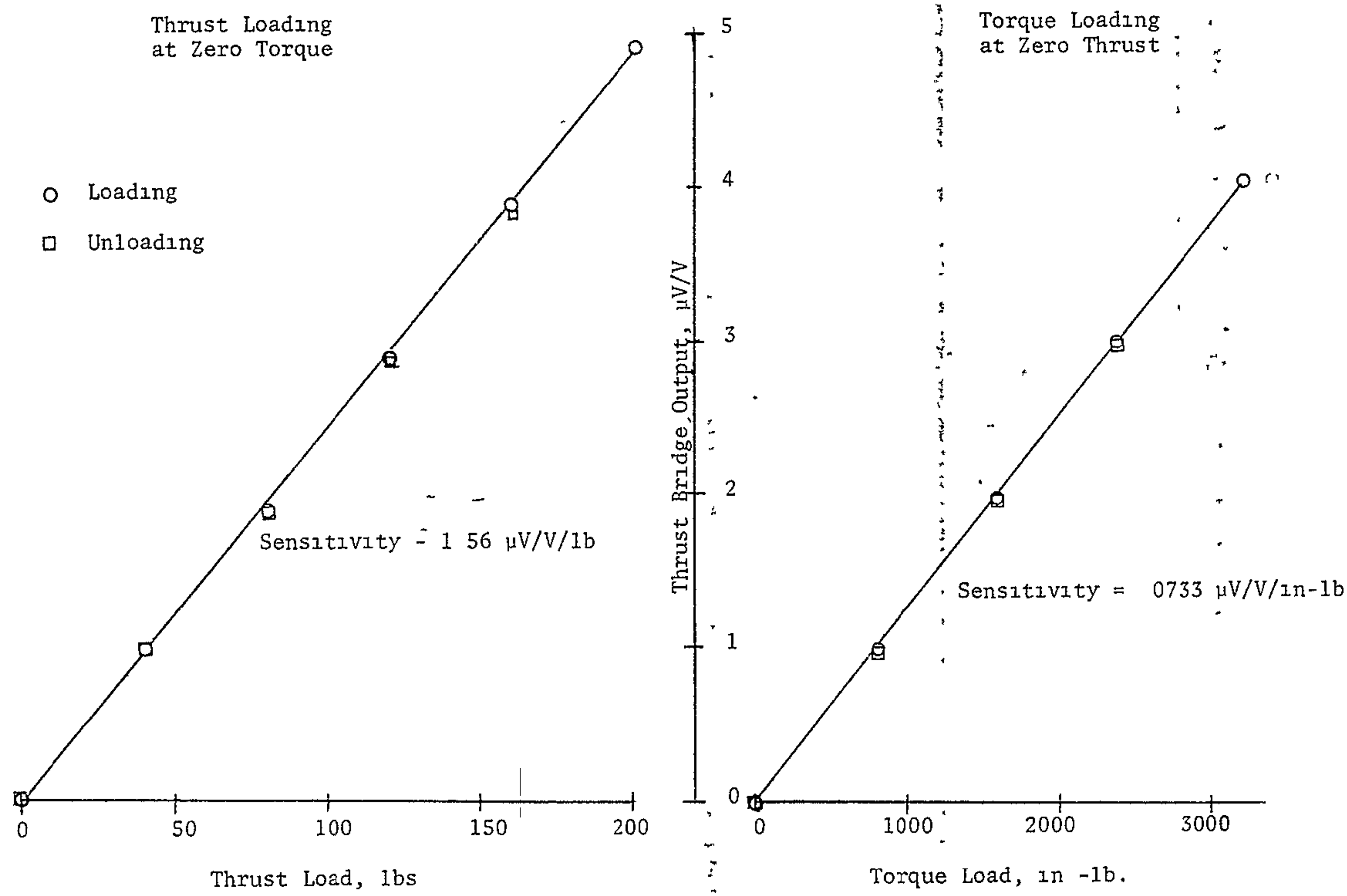

3-30

Figure 3.12 Semi-Conductor Thrust Bridge Calibration

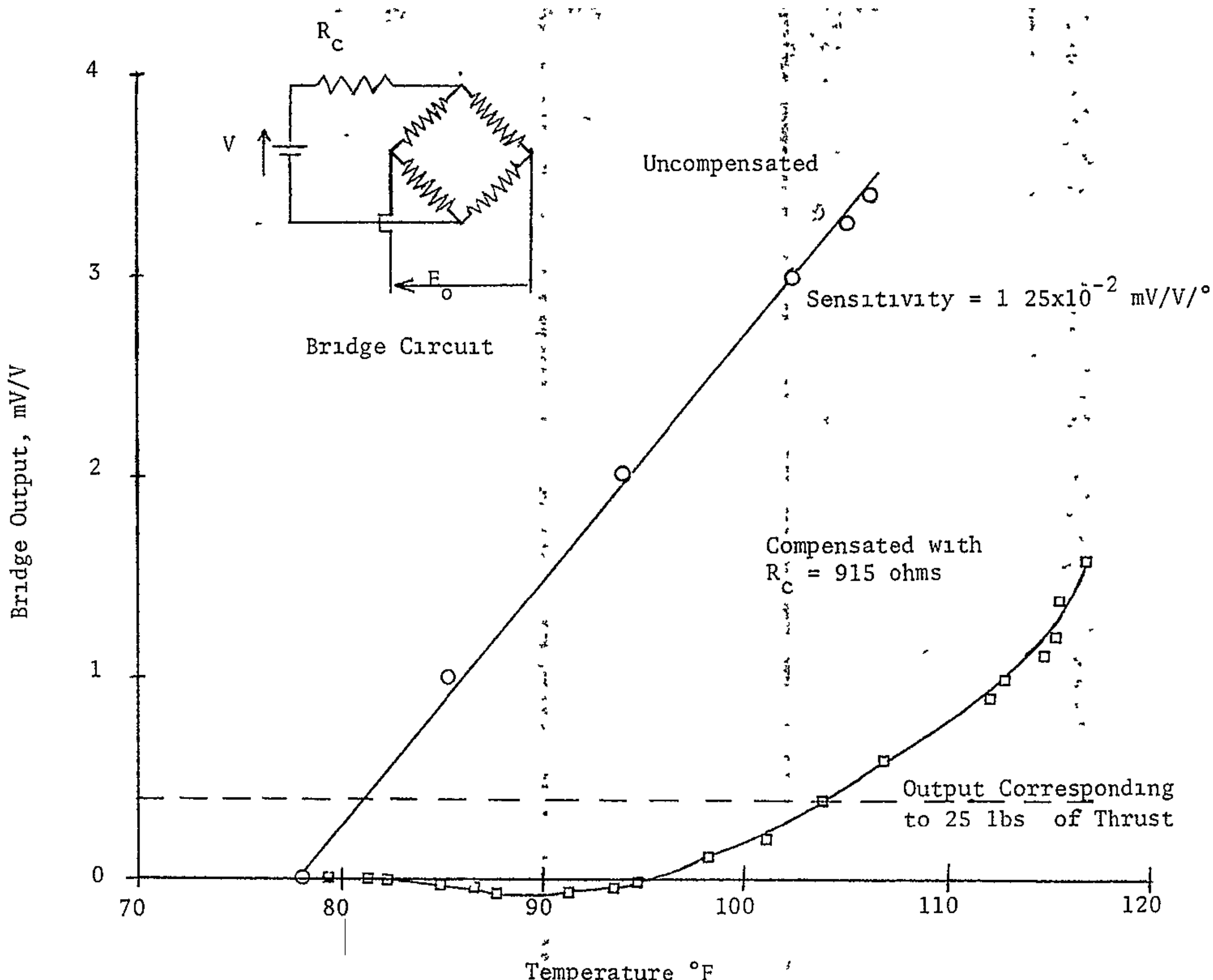

Figure 3 13 Temperature Compensation of the Semi-conductor Thrust Bridge

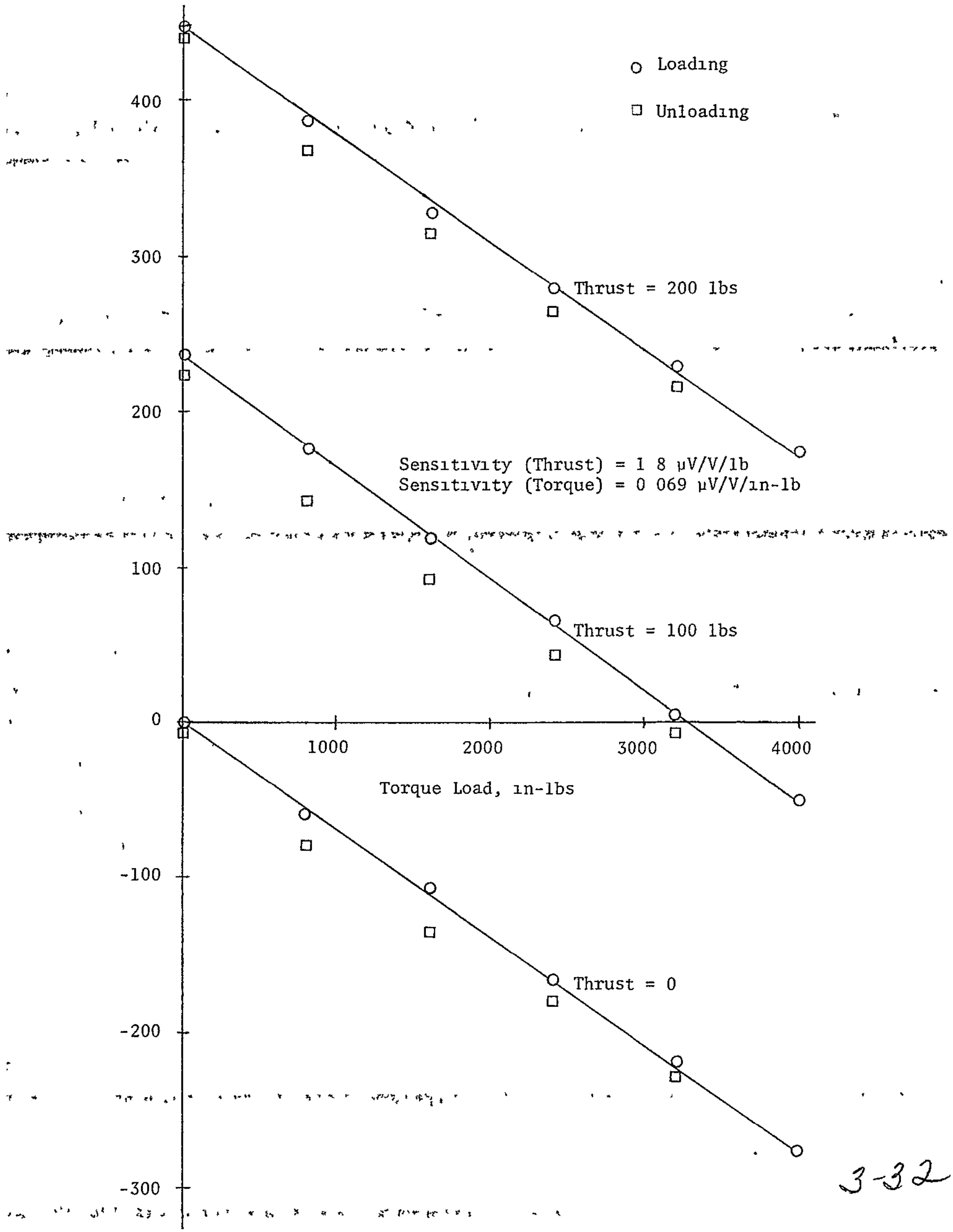

3-32

Figure 3 14 Semi-Conductor Thrust Bridge Calibration for Torque Interaction

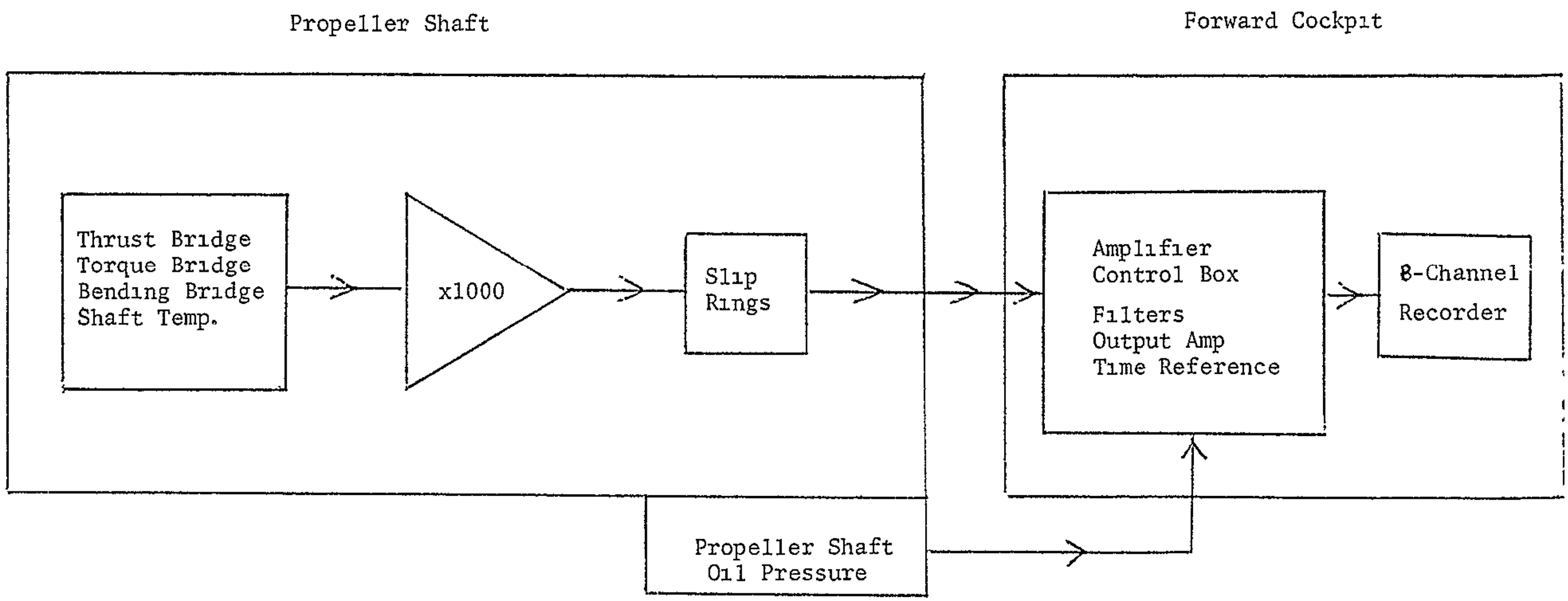

Figure 3 15 Block Diagram of In-Flight Instrumentation System

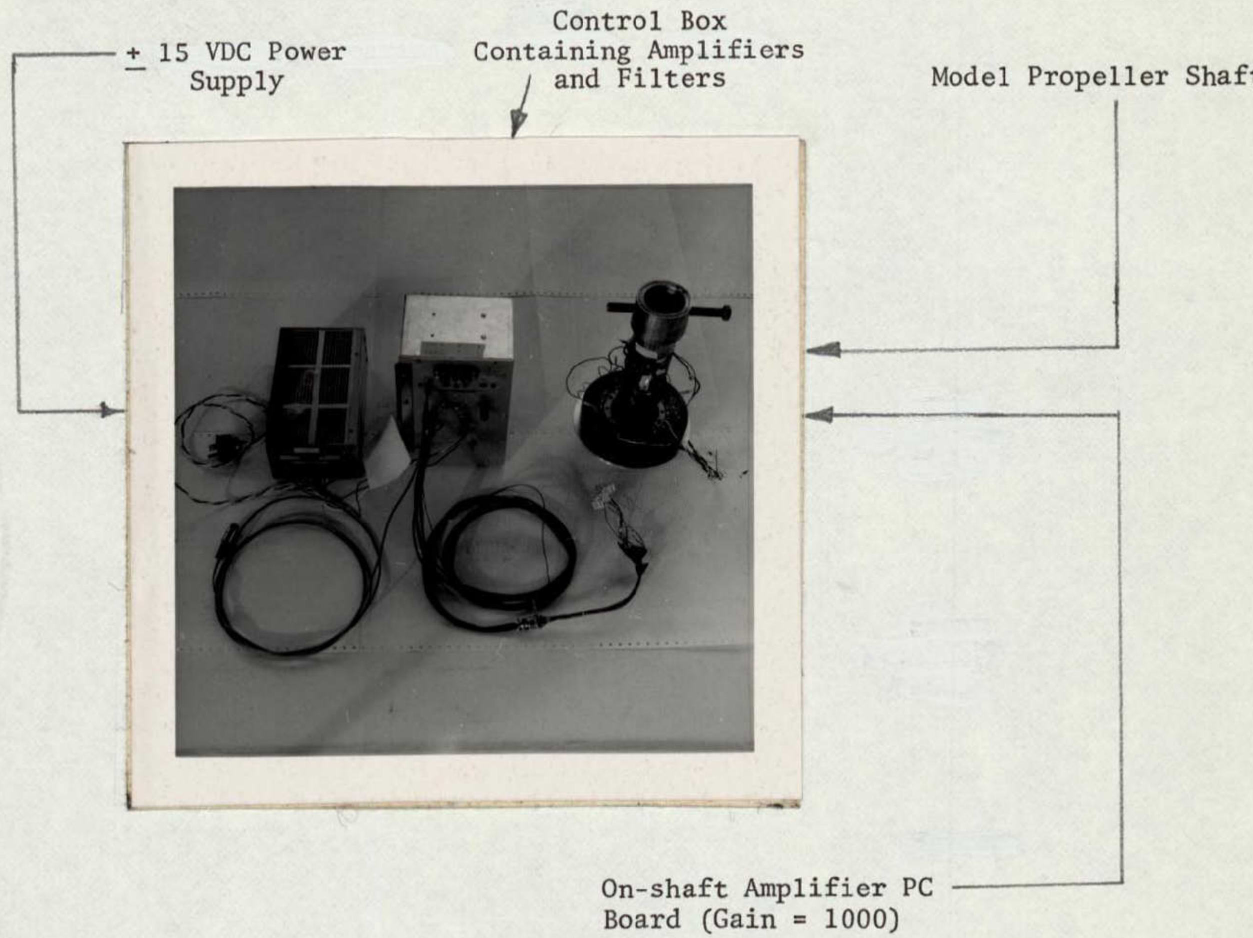

Figure 3.16 The Instrumentation System

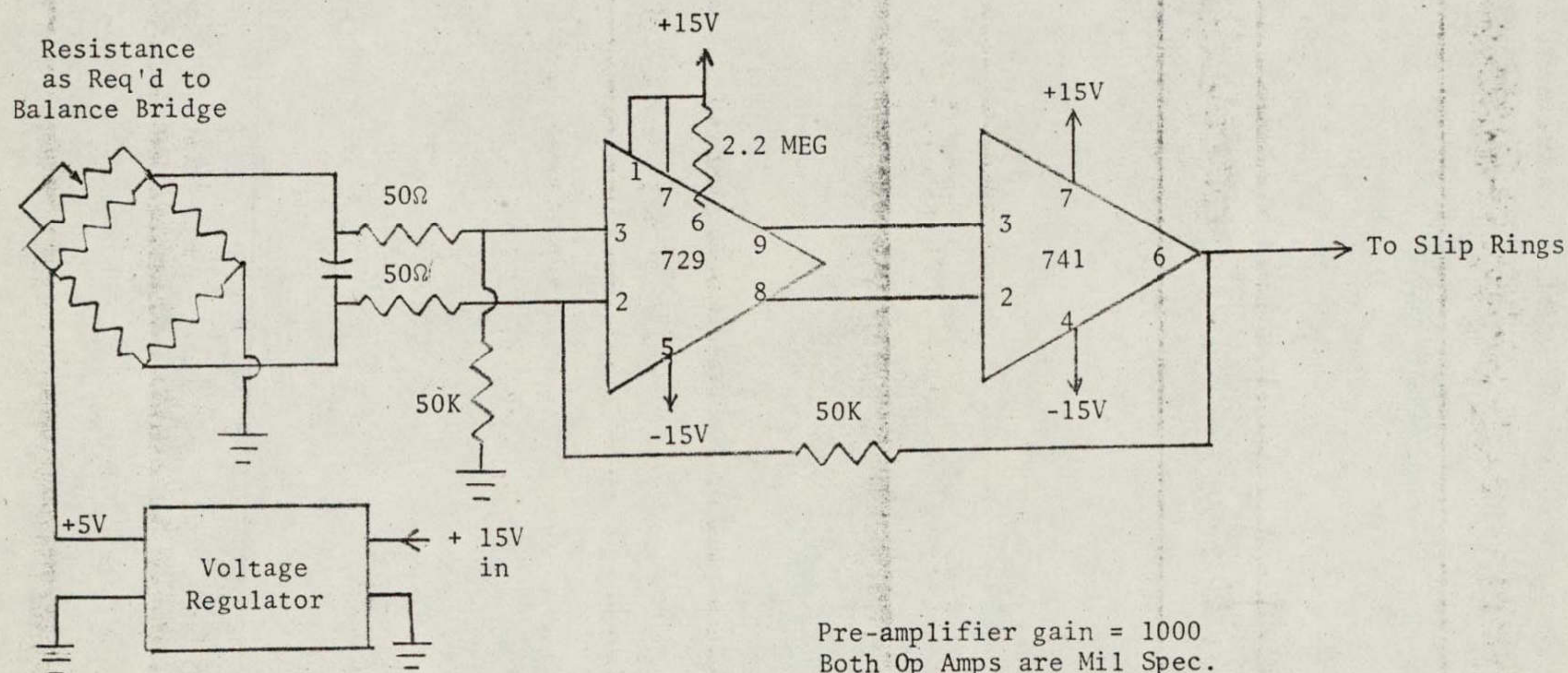

Figure 3.17 Schematic of One Typical Channel of On-Shaft Instrumentation

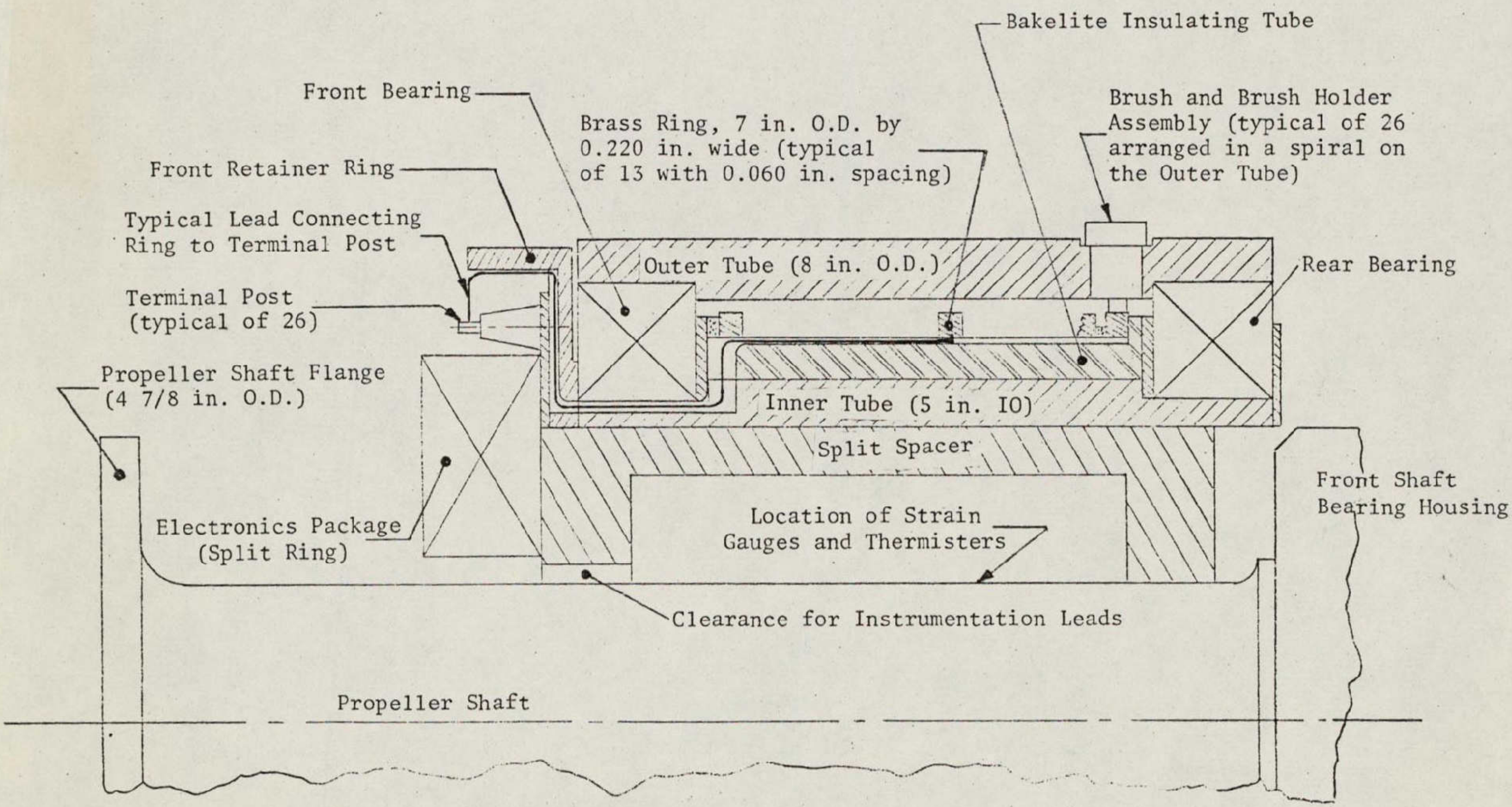

Overall Length (including electronics package) = 7.3 inches

Figure 3.18 Sectional Sketch of Slip Ring Assembly.

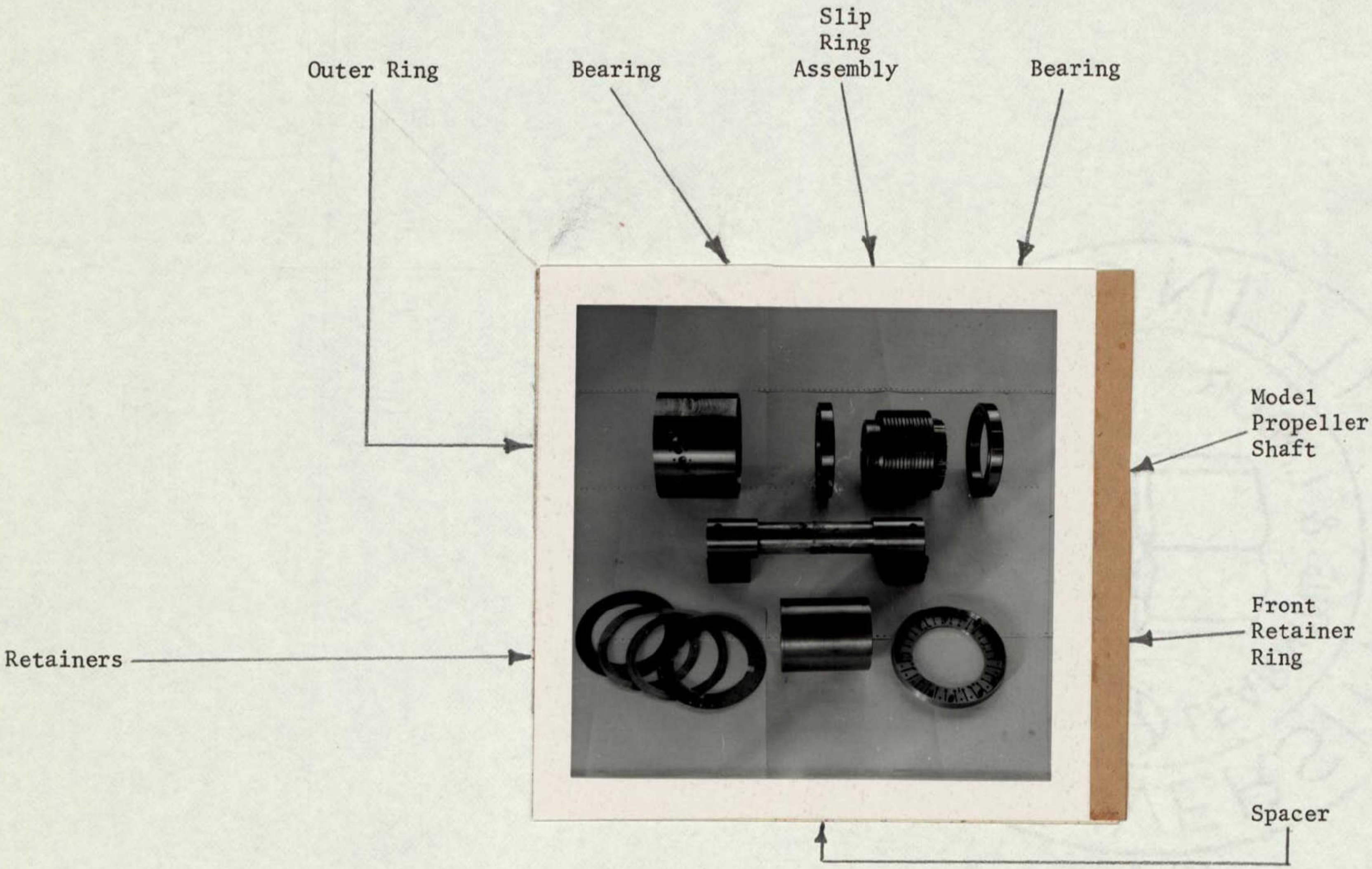

Figure 3.19 The Slip Ring Assembly

Maximum Load	Section Characteristics	Strength of Section	Strain Equation	Strain Per Unit Load & Maximum Strain	Stress Per Unit Load & Maximum Stress
Thrust T_{Max} = 500 lb	$A = 1\ 89\ in^2$	$AE =$ $5\ 68\times10^7$ lb	$\varepsilon_T = \frac{T}{AE}$	$\frac{\varepsilon_T}{T} = 0177$ micro-strains/lb $\varepsilon_{T_{Max}} = 8\ 85$ micro-strains	$\frac{\sigma_T}{T} = 529\ in^{-2}$ $\sigma_{T_{Max}} = 265$ psi
Torque Q_{Max} = 14,000 in-lb	$J = 2\ 06\ in^4$	$JG =$ $2\ 2\times10^7$ in^2-lb	$\varepsilon_Q = \frac{QR}{2JG}$	$\frac{\varepsilon_Q}{Q} = 0268$ micro-strains/ in-lb $\varepsilon_{Q_{Max}} = 375$ micro-strains	$\frac{\sigma_Q}{Q} = 573\ in^{-3}$ $\sigma_{Q_{Max}} = 8020$ psi
Bending M_{Max} = 1500 in-lb (at bearing end of the shaft)	$I = 1\ 03\ in^4$	$IE = 3\ 09\times10^7$ in^2-lb	$\varepsilon_B = \frac{MR}{IE}$	$\frac{\varepsilon_M}{M} = 0382$ micro-strains/ in-lb $\varepsilon_{M_{Max}} = 58\ 5$ micro-strains	$\frac{\sigma_B}{M} = 1\ 14\ in^{-3}$ $\sigma_{B_{Max}} = 1718$ psi

TABLE I

PROPELLER SHAFT LOADS

Sensor Arrangement	$d\varepsilon/dT$	Full Scale $\varepsilon_{T_{Max}}$	$d\varepsilon/dQ$	Full Scale $\varepsilon_{Q_{Max}}$	% Interaction $\frac{\varepsilon_{Q_{Max}}}{\varepsilon_{T_{Max}}} \times 100$	Error and Remarks
Mech Strain Intensifier I	.15 μV/V/lb	75 μV/V	.045 μV/V/in-lb	630 μV/V	840%	Hysterisis Fair Repeatability Sensitive to pre-load Large Torque Inter-action
Mech Strain Intensifier II	25 μV/V/lb	125 μV/V	019 μV/V/in-lb	266 μV/V	212%	Hysterisis Fair Repeatability Sensitive to pre-load Large Torque Inter-action
Foil Bridge on Shaft	024 μV/V/lb	12 0 μV/V	00081 μV/V/in-lb	11 34 μV/V	94%	Low signal-to-noise Hysterisis No Temperature problem Torque Interaction
Semi-Cond Bridge on Shaft	1.56 μV/V/lb	780 μV/V	0733 μV/V/in-lb	1.027 mV/V	132%	High signal-to-noise Good repeatability Torque Interaction Temperature problems
Torque Bridge on Shaft	---	40 micro-strains 20 μV/V	12 micro-strains/in-lb	1680 micro-strains 840 μV/V	< 2 5%	Good repeatability High signal-to-noise Negligible thrust interaction No temperature problems

TABLE II

SENSOR EVALUATION TEST RESULTS

APPENDIX A

NUMERICAL ANALYSIS OF PROPELLERS

by R. M. Plencner

LIST OF SYMBOLS

a	axial interference factor
a'	rotational interference factor
A_n	coefficients of sine series
AR	aspect ratio
B	number of blades
c	non-dimensional chord, C/R
C	chord, feet
C_L	lift coefficient
C_D	drag coefficient
D	diameter, feet
I	induction factor
J	advance ration, V/nD
k	loading factor
n	rotational speed, rev/sec
Q	torque, ft-lbs
Q_c	torque coefficient
r	distance along blade, feet
R	radius of propeller, feet
$\overline{s}$	vector from origin to segment of trailing vortex filament
$\overline{t}$	vector from origin to a blade section
T	thrust, lbs
T_c	thrust coefficient
v	velocity induced at the propeller disk, ft/sec
V	forward velocity of propeller, ft/sec

w_n	normal induced velocity
W	vector sum of rotational and forward velocities
X	non-dimensional distance along blade, r/R
Z	rearward distance from the propeller, feet
α_g	absolute geometric angle of attack
α_i	induced angle of attack
α_o	effective or sectional angle of attack
β	blade angle
Γ	circulation
δ	interval around the singularity
η	efficiency
θ	parametric variable of the helix, radians
λ	tip speed ratio, $V/\Omega R$
ρ	density, slugs/ft^3
σ	propeller solidity, $BC/2\pi r$
ϕ	angle between the relative velocity and the horizontal plane
Ω	rotational speed, rad/sec

I. INTRODUCTION

A great deal of effort and expertise went into modeling the aerodynamic characteristics of propellers in the early part of this century, However, with the coming of the jet age in the early 1950's, the propeller was made obsolete for many applications and new theoretical work on propeller theories was almost non-existent Therefore, most of the work done in this area was undertaken before digital computers were developed Since the problem of flow around a propeller is by nature very complex, these early approaches to the problem necessitated many simplifying assumptions and often made use of graphical techniques to obtain solutions to the problem

Recent years have seen a renewed interest in propeller modeling for predicting their performance in a wide variety of applications These applications include more efficient propellers to reduce fuel consumption, propellers suitable for STOL aircraft, low noise propellers for commercial and general aviation aircraft, as well as rotors for wind mills. Many of the applications require more accurate prediction over a wider range of operating conditions than is possible with classical propeller theories

The purpose of this paper is to review the classical approaches to the propeller problem and then dispense with as many simplifying assumptions as possible in order to produce a theory that more closely models the actual physical phenomenon

II. CLASSICAL THEORIES

Momentum Theory - A propeller produces thrust by increasing the velocity of a large quantity of air. This production of thrust is associated with a loss of energy which is due to the increase in kinetic energy, rotational motion imparted by the torque and frictional losses of the propeller blades In the simplest form of the momentum theory, first set forth by R E Froude [1] and W. J. Rankine [2], only the axial component of momentum is considered; the rotational and frictional losses are ignored. Therefore, the theory describes the characteristics of in ideal propeller.

The axial momentum theory is developed [3, 4] by replacing the propeller with a propeller disk that has an infinite number of blades, and the thrust uniformly distributed over the disk. The flow is assumed to be incompressible and irrotational in front of and behind the propeller disk. Under these conditions the change in pressure across the propeller disk is equal to the total pressure head in front of the disk minus the total pressure head behind the disk. It can then be shown that at the propeller disk the increase in velocity over the free stream value is one half of the increase in the ultimate wake. The efficiency which is predicted by the momentum theory, which is the maximum theoretical efficiency, is given by

$$\eta = \text{propeller efficiency} = \frac{V}{V+v} \quad (1)$$

where V is the free stream velocity and v is the velocity increase at the propeller disk.

Practical applications of the momentum theory are limited due to the gross simplifications that are made The theory neglects rotational energy losses, non uniform thrust loading losses, profile drag, blade interference, and compressible drag changes Its direct application, therefore, is only principally useful in obtaining an upper limit on efficiency or a crude first estimate for the performance of a propeller. A more general form of the momentum theory [5] includes rotational momentum as well as axial momentum. However, this added complexity does not increase its usefulness in most applications.

Blade Element Theory - The blade element theory [5] analyzes the aerodynamic characteristics of the propeller by estimating the aerodynamic forces experienced by each blade element as it moves through the air. The blade element theory is evolved by assuming that the aerodynamic forces acting on a given blade element are equivalent to the forces acting on a suitable finite wing of the same airfoil section moving linearly with the same relative velocity and the same geometric angle of attack that is experienced by the propeller blade section. The contributions from all the blade elements may be added up using a strip integration technique to get the overall propeller characteristics. From the geometry of Figure 1 it can be shown that the incremental thrust and torque of any blade element operating at a geometric angle of attack, $\alpha_g = \beta - \phi$, are given by

$$\frac{d\Gamma}{dr} = \frac{1}{2} BC\rho W^2 \left(C_L \cos\phi - C_D \sin\phi\right) \tag{2}$$

and

$$\frac{dQ}{dr} = \frac{1}{2} BC\, r\rho W^2 \left(C_L \sin\phi + C_D \cos\phi\right) \tag{3}$$

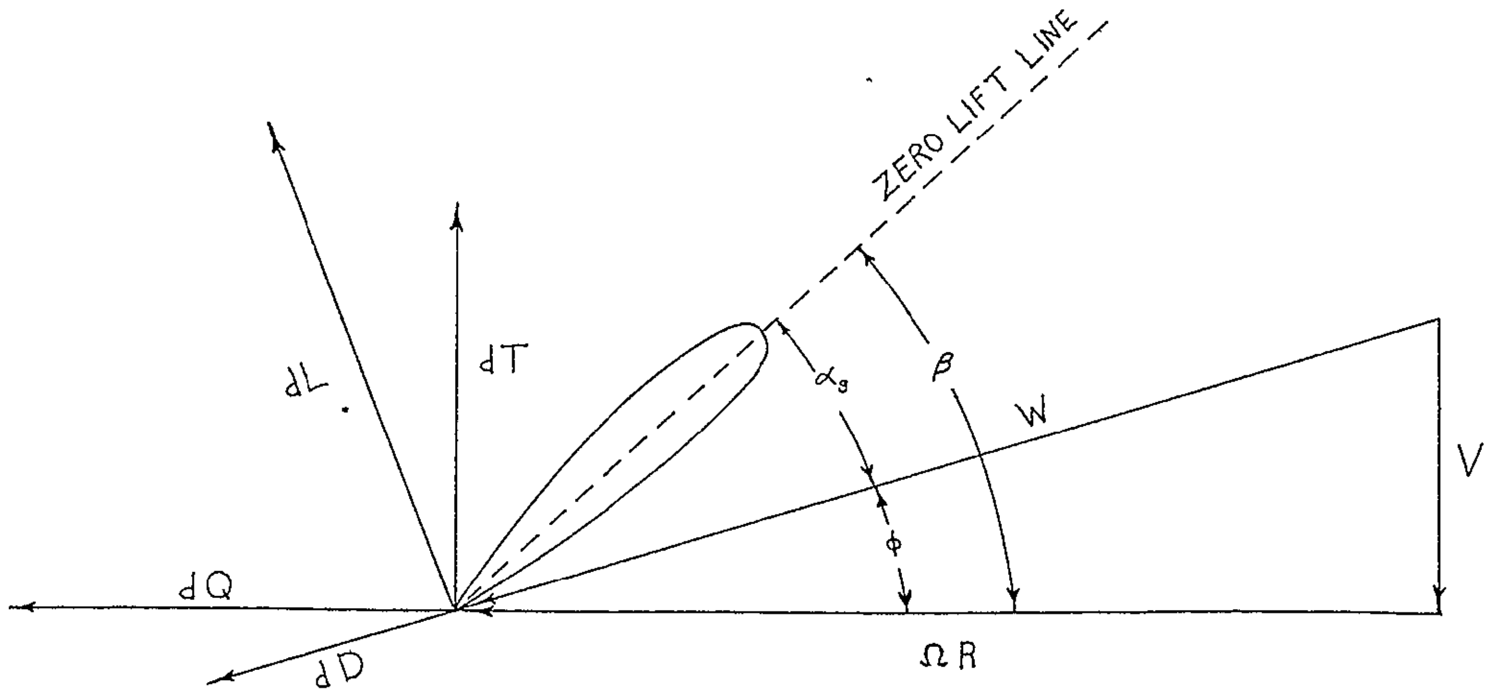

Figure 1. Force and velocity diagram for the blade element theory

where $W^2 = V^2 + \Omega^2 r^2$. The validity of equations (2) and (3) is largely dependent on the characteristics of the wing used to represent the propeller blade section In order to accurately account for the interference effects, the characteristics of the assumed wing would have to change from station to station However, the blade element theory greatly simplifies the problem by assuming the wings used to represent the blade element sections have an aspect ratio of six. Thus the problem is completely specified by equations (2) and (3) when the chord and blade angle distribution and the aerodynamic characteristics of an aspect ratio six wing of the same airfoil section as the blade element are known.

The blade element theory better takes account the effect of the geometric shape of the propeller than does the momentum theory. However, it still fails to accurately account for the interference velocities induced by the trailing vortex system.

Vortex Theory - The vortex theory of propellers is basically a combination of the momentum theory and the blade element theory. Therefore, it is often referred to as the blade element-momentum theory: To avoid confusion with other theories it will be referred to as the Glauert vortex theory [5, 6, 7] in this paper. The Glauert theory is based on the assumption that the trailing vortex filaments which are produced by the rotating blades form helical vortex sheets as they pass downstream. An exact application would require the induced velocity produced by the trailing vortex system to be computed at each blade station. However, Glauert simplified the problem by assuming the propeller to have an infinite number of blades. This assumption removes the periodicity of the flow, therefore, the velocity for any given radius is constant over the propeller disk. As a result, the momentum theory may be used to evaluate the interference velocities. The geometry of the problem is given in Figure 2 a and a' are defined as the axial and rotational interference factors respectively $V(1 + a)$ is the forward velocity, V, plus the axial interference velocity. $\Omega r(1 - a')$ is the angular velocity of the propeller blade section minus the rotational interference velocity. The effective velocity, W_r, of the blade element is just the vector sum of $V(1 + a)$ and $\Omega r(1 - a')$. From the geometry given in Figure 2 the following relations may be defined

$$W \sin \phi = V(1 + a) \tag{4}$$

$$W \cos \phi = \Omega r(1 - a') \tag{5}$$

It is often convenient to define a non dimensional speed ratio, λ, as the forward speed divided by tip speed. Using equations (4) and (5) the speed ratio may be written in terms of the interference factors as,

$$\lambda = \frac{V}{\Omega R} = \frac{1 - a'}{1 + a} \tan \phi \tag{6}$$

The equation for the elemental thrust and torque are found in the same manner as for the blade element theory, except now they are written in terms of the interference factors and are given in non-dimensional form as,

$$R \frac{dT_c}{dr} = \sigma \left(\frac{r}{R}\right)^3 (1 - a')^2 (C_L \cos \phi - C_D \sin \phi) \sec^2 \phi \tag{7}$$

and

$$R \frac{dQ_c}{dr} = \sigma \left(\frac{r}{R}\right)^4 (1 - a')^2 (C_L \sin \phi + C_D \cos \phi) \sec^2 \phi \tag{8}$$

where the non dimensional thrust and torque coefficients are defined by

$$T = T_c \pi R^4 \rho \Omega^2 \tag{9}$$

and

$$Q = Q_c \pi R^5 \rho \Omega^2 \tag{10}$$

respectively Equations (6), (7), and (8) are not sufficient to determine

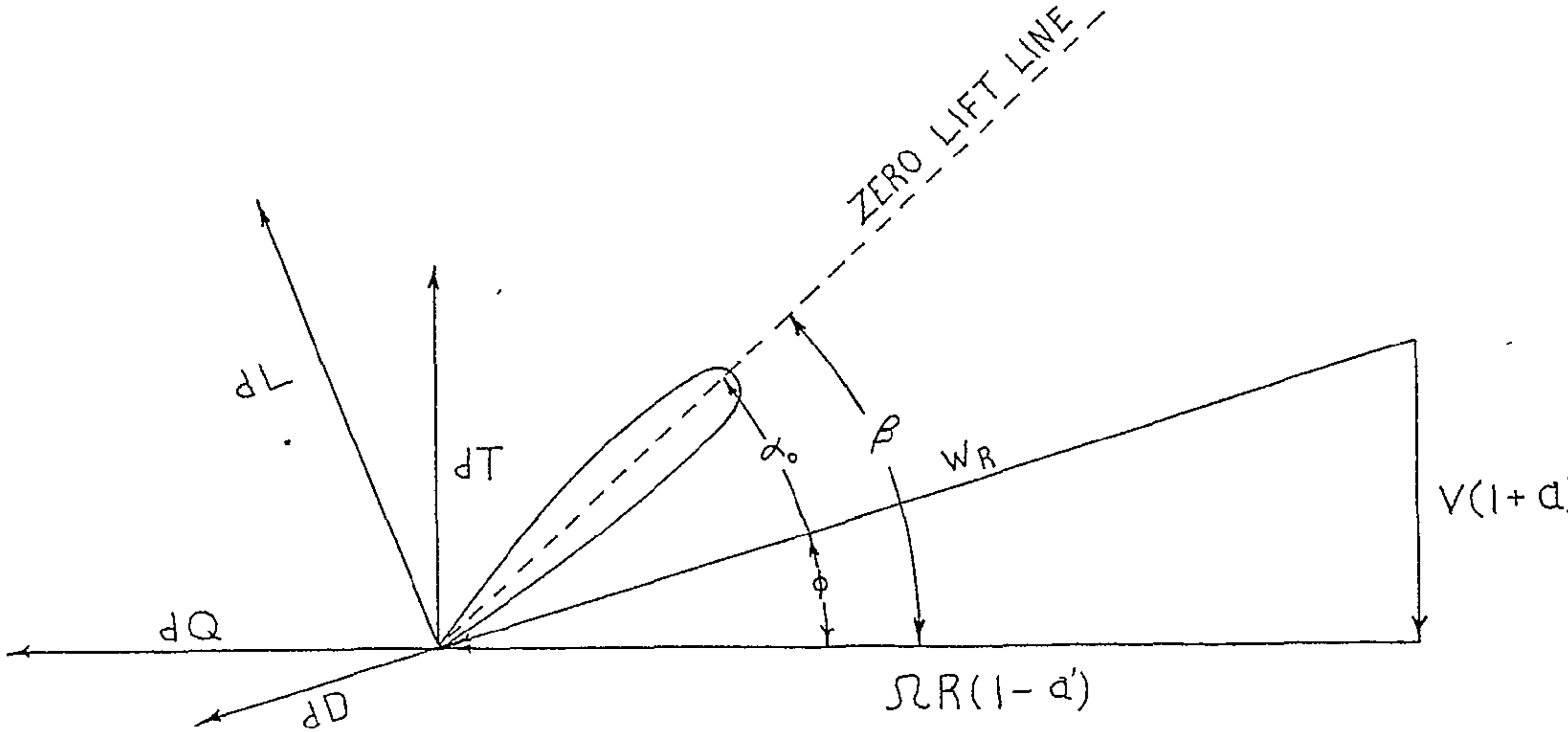

Figure 2. Force and velocity diagram for Glauert vortex theory

the interference factors a and a'. It is now necessary to make use of the assumption of an infinite number of blades. This makes it possible to apply the momentum theory to obtain relations needed to evaluate a and a'. The results of the axial momentum theory, where rotational momentum is neglected, can be used to determine the axial interference factor as

$$\frac{a}{1 + a} = \frac{\sigma(C_L' \cos \phi - C_D \sin \phi)}{4 \sin \phi} \tag{11}$$

Equation (11) is not exact. In addition to neglecting the flow periodicity due to a finite number of blades, it also is based on the assumption of no slip stream contraction, and no rotational velocity component. The rotational interference factor may be evaluated by equating the torque to the rate of increase of angular momentum. This relation may be written in terms of the rotational interference factor as,

$$\frac{a'}{1 - a'} = \frac{\sigma(C_L \sin \phi + C_D \cos \phi)}{4 \sin \phi \cos \phi} \tag{12}$$

Equations (6), (7), (8), (11), and (12) are sufficient to determine the thrust and torque of a given propeller when the number of blades, the chord distribution, blade angle variation and the aerodynamic characteristics of the airfoil used at each blade location are known.

Due to the assumptions made, the above set of equations accurately apply only to a lightly loaded propeller with a large number of blades. However, reasonable results may be obtained for many conditions varying greatly from the above restrictions The predicted thrust and torque distributions along the blade differ from the actual distributions for propellers operating at high blade loadings or for propellers with square tipped blades In the case of square tipped blades, the vortex theory fails to predict the fact that the thrust must fall to zero at the tip [8].

Goldstein's Theory - Goldstein [9] dispenses with the assumption that the spacing between successive trailing vortex sheets is small and assumes there is a bound vortex filament springing from each blade element The local strength of the trailing sheet is the negative of the circulation gradient around the corresponding blade section The circulation must fall to zero at the root and the tip These trailing vortex filaments approximately follow a helical path in the slip stream All the filaments together form a helicoidal surface. Goldstein specifically considers the optimum circulation distribution for which the energy lost due to the production of the trailing vortex system is a minimum, for a given thrust. Betz proved for lightly loaded propellers that this optimum circulation distribution corresponds to the requirement that the vortex sheet move rearward as if it were a rigid helicoid. Thus, the flow in the wake between the helicoidal surfaces is that of an inviscid, continuous, irrotational fluid, with zero circulation The circulation around a given blade element is equal to the discontinuity in the velocity potential of the respective point on the helicoidal vortex surface Since the problem is one of potential flow, it is possible to apply Laplace's equation,

$$\nabla^2 \phi = 0 \tag{13}$$

where ϕ is the velocity potential. Using the relations

$$\zeta = \theta - \frac{\Omega z}{V} \tag{14}$$

and

$$\mu = \frac{\Omega r}{V} \tag{15}$$

Laplace's equation in polar coordinates may be transformed to a more convenient form given by,

$$\mu^2 \frac{\partial^2\phi}{\partial\mu^2} + \mu\frac{\partial\phi}{\partial\mu} + (1 + \mu^2) \frac{\partial^2\phi}{\partial\zeta^2} = 0 \tag{16}$$

The boundary condition for the problem becomes,

$$\frac{\partial\phi}{\partial\zeta} = - \frac{\Omega^2 r^2}{V^2+\Omega^2 r^2} \frac{wV}{\Omega} \tag{17}$$

for $\zeta = 0$ or π and $0 \le r \le R$. In addition, ϕ must be continuous everywhere except at the helicoidal vortex surface, and its derivative must vanish when r is infinite. Goldstein goes through a rigorous solution of this problem to obtain the loading factor, k, which is just a non-dimensional circulation defined by

$$k = \frac{\Gamma B}{2w \pi r \tan \phi} \tag{18}$$

Lock [10] applied Goldstein's solution to a method for predicting the characteristics of an arbitrary propeller. The development of this method parallels that of the Glauert vortex theory quite closely, except that Goldstein's solutions are used to determine the interference velocities at the blades The equations that are obtained for the interference factors are

$$\frac{a}{1 + a} = \frac{\cos^2\phi}{k} \frac{\sigma C_L \cos \phi - C_D \sin \phi}{4 \sin^2 \phi} \tag{19}$$

and

$$\frac{a'}{1 - a'} = \frac{\cos^2 \phi}{k} \frac{\sigma C_D \cos \phi + C_L \sin \phi}{4 \sin \phi \cos \phi} \tag{20}$$

Equations (19) and (20) differ from equations (7) and (8) of the Glauert vortex theory by the factor $\frac{\cos^2\phi}{k}$ It should be noted that in the limit when the number of blades goes to infinity.

$$k = \cos^2 \phi \tag{21}$$

Thus, equations (19) and (20) reduce to the Glauert vortex theory, equations (7) and (8), for the case of an infinite number of blades.

Goldstein's loading factor, k, only applies exactly when there is a particular distribution of circulation along the blade to give optimum loading as defined in Goldstein's original problem. However, Lock shows that equations (19) and (20) make adjustments for tip losses and are generally more accurate than the Glauert vortex theory formulae, especially in the case of a square tipped blade.

Theodorsen's Theory - Theodorsen [11, 12, 13, 14, 15, 16] attacks the same problem of the optimum propeller as was developed by Goldstein. However, Theodorsen expanded and extended the results of Goldstein's work Betz's requirement that the trailing vortex sheet move rearward as a rigid vortex sheet for an optimum loaded propeller was proved only for a lightly loaded propeller Theodorsen extended the interpretation of these results to apply to heavy loadings.

Goldstein's original solution also applied only to infinitely light loadings Theodorsen showed that it is possible to extend these results to heavy loadings by including the rearward displacement velocity of the helicoidal vortex surface and doing all the calculations in the wake infinitely far behind the propeller This does not change the potential problem that must be solved. However, it does change the operating conditions which a given solution corresponds to. Including the rearward displacement velocity of the vortex surface, instead of assuming it to be negligibly small, takes account of the contraction of the slip stream.

Theodorsen's method depends on the solution for the propeller loading coefficient, k, which is a function of the distribution of circulation along the blade. Goldstein's results may be used to evaluate the loading coefficient. However, Goldstein was only able to obtain a small number of solutions. Therefore, Theodorsen used an electrical analogy method to experimentally measure the loading function By using the electrical analogy, he was able to obtain the loading function for dual rotating propellers as well as for single propellers. The drawback of this method is that one is limited to the charts and tables which Theodorsen gives for the loading function.

Application of the Prandtl Theory - Lock [17, 18, 19, 20] put forth a theory which solved the propeller problem through an application of the Prandtl theory [21] for a monoplane wing In calculating the induced velocity along the blade, the actual helicoidal trailing vortex sheets are replaced with a system of vortices in two-dimensions. This method assumes that the flow around the helicoidal vortex sheets can be approximated by the flow around a system of parallel two-dimensional vortex sheets whose strength is equal to the actual strength of the helical vortices at the same radial distance from the axis of rotation. The distance between successive sheets is equal to the pitch of the airscrew The Fourier series may then be used to represent any arbitrary distribution of vorticity with radius Strict application of this theory would require the coefficients of the Fourier series to be found in a manner analogous to that employed in wing theory, where a system of simultaneous equations in the coefficients must be solved. However, to simplify the technique, a graphical method is applied to determine the coefficients of the series and corrections are then applied to account for errors introduced by replacing the helicoid vortex sheet by a system of two-dimensional plane laminae The method in its final form is strictly a graphical technique, using charts developed by Lock

Moriya Theory - Moriya [22] developed a calculation method for the aerodynamic characteristics of a propeller in which he obtained the induced velocity by introducing an induction factor, I To obtain the induction factor it is assumed that the trailing vortices springing from each blade form a helicoidal surface which extends rearward from the blade to infinity The downwash velocity at each blade element due to the whole vortex system is then calculated by application of the Biot-Savart law The downwash integral becomes singular when calculating the velocity induced at a point where the trailing vortex filament springs from that same point. If the vortex filament were straight instead of helical, it would exhibit the same singular behavior Therefore, Moriya introduced an induction factor, I, which defined as,

$$I = \frac{d\ w_n}{d\ w_{n_1}} \tag{22}$$

where $d\ w_n$ is the normal velocity induced by a helical vortex filament and $d\ w_{n_1}$ is the normal velocity induced from a straight vortex filament At the point where the vortex filament leaves the blade, the induction factor takes on the value of unity Induction factors for various advance ratios were calculated graphically by Moriya and are tabulated in reference [22]

A successive approximation scheme to determine the aerodynamic characteristics of an arbitrary propeller was developed by Moriya In this scheme the circulation around each blade element is calculated corresponding to an equivalent monoplane wing of aspect ratio six Using this calculated circulation distribution and the suitable induction factors, the normal velocity at each station is obtained by graphically integrating the following.

$$w_n = \int_0^1 \frac{\frac{d\Gamma}{dx}}{4 \pi R} \quad \frac{I}{x - x'} \; dx \qquad (23)$$

An equivalent aspect ratio for each blade section can then be calculated from

$$\frac{w_n}{V} = \frac{C_L}{\pi AR} \qquad (24)$$

This scheme is repeated by calculating the circulation distribution corresponding to the new equivalent aspect ratio at each blade element This iteration is repeated until the equivalent aspect ratios of two successive approximations are sufficiently close The lift and drag coefficients are found in the final iteration and are used in the normal strip theory formulas, equations (2) and (3), to find the thrust and torque coefficients It is reported by Moriya that only one or two iterations are needed to obtain a good degree of accuracy

III THEORETICAL INVESTIGATION

Most of the preceding theories involve many simplifying assumptions to obtain the interference velocities needed to analyze the aerodynamic characteristics of a propeller The equations and method needed to solve for the induced velocities with a minimum of simplifying assumptions in a manner analogous to that of finite wing theory will now be developed. The basic assumption is that of a helicoidal trailing vortex sheet which extends rearward from the blade to infinity. The velocity induced by a segment, $\overline{d\ell}$, of a trailing vortex filament can be calculated at each blade section by means of the Biot-Savart law which is given as,

$$\delta v (r) = \frac{\Gamma}{4 \pi} \frac{\overline{d\ell} \times \overline{(t-s)}}{|t-s|^3} \tag{25}$$

where t is the vector from the origin to the blade section at which the induced velocity is to be calculated and s is the vector from the origin to the vortex filament segment $\overline{d\ell}$. For the geometry depicted in Figure 3 the following relations can be written,

$$\overline{t} = R x' \hat{i} \tag{26}$$

$$\overline{s} = R x \cos \theta \hat{i} + Rx \sin \theta \hat{j} + Ra \tan \phi \hat{k} \tag{27}$$

$$\overline{d\ell} = R x \sec \phi \, d\theta \, [- \cos \phi \sin\theta \hat{i} + \cos \phi \cos \theta \hat{j} + \sin \phi \hat{k}] \tag{28}$$

The induced velocity at a point x' due to a semi-infinite vortex filament springing from the point x on the blade is found by substituting equations (26), (27) and (28) into equation (25) and then integrating this equation over θ from zero to infinity The normal component of this induced velocity is given as,

$$dw_n = \frac{\Gamma}{4\pi R} \int_0^\infty \frac{x[x^2 - xx' \cos \theta] + [x(\theta \sin \theta + \cos \theta) - x'] \lambda^2}{[x'^2 - 2 xx' \cos \theta + x^2 + \theta^2 \lambda^2]^{3/2} \; [\lambda^2 + x'^2]^{1/2}} \, d\theta \tag{29}$$

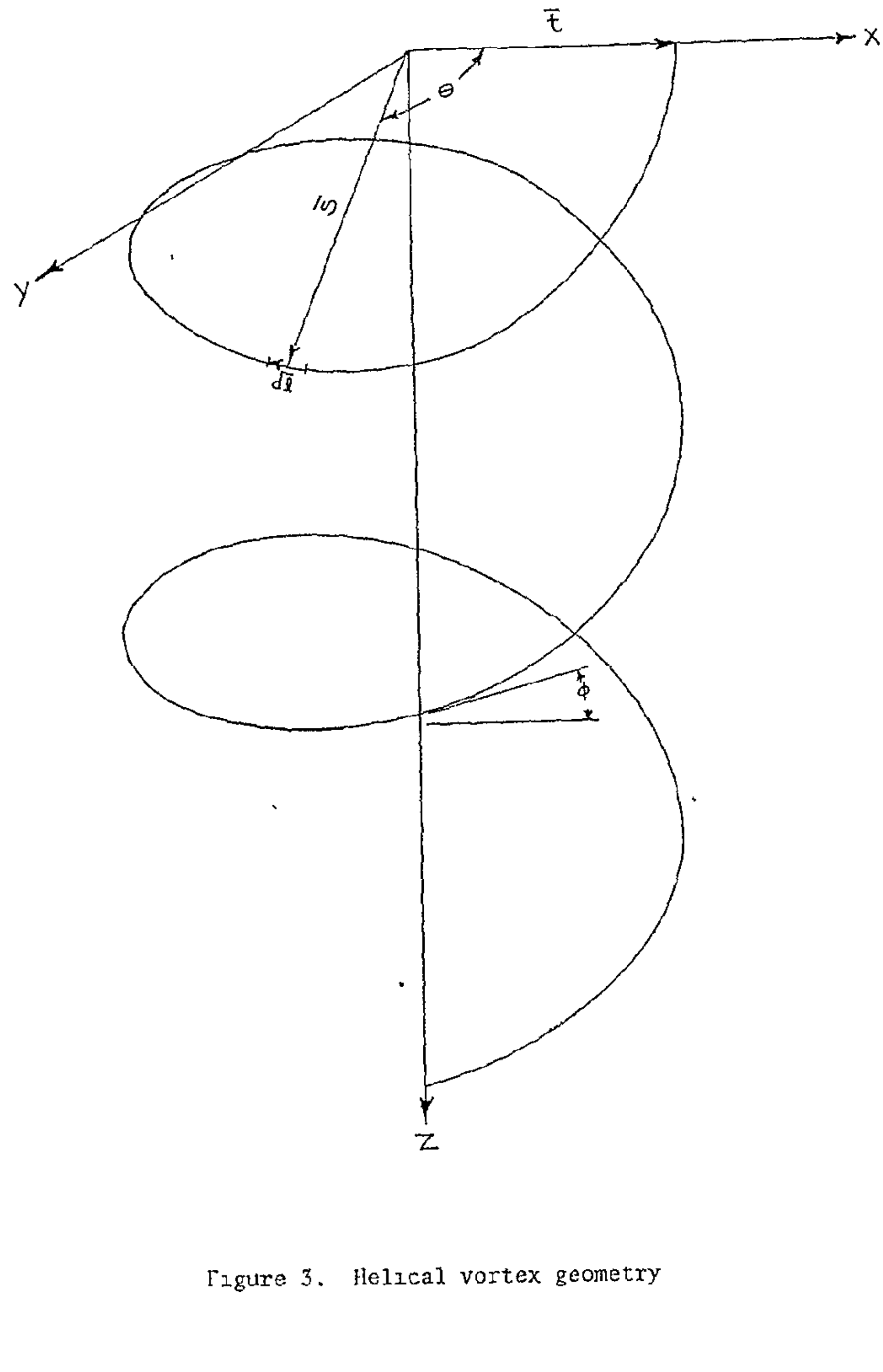

Figure 3. Helical vortex geometry

The normal induced velocity at the point x' due to the vortex filaments springing from the radius x on all the blades is

$$dw_n = \frac{d\Gamma}{4\pi R} \sum_{k=1}^{B} \int_0^\infty \frac{[x^2 - xx' \cos \theta_k]x' + [x(\theta \sin \theta_k + \cos \theta_k) - x'] \lambda^2}{[x'^2 - 2xx' \cos \theta_k + x^2\lambda^2]^{3/2} [\lambda^2 + x'^2]^{1/2}} d\theta \quad (30)$$

where $\theta_k = \theta + \frac{2\pi (B-k)}{B}$

The normal induced velocity at some point x' due to all the vortex filaments springing from each of the blades is found by integrating equation (30) over the blade and can be expressed as

$$w_n(x') = \int_0^1 \frac{\frac{d\Gamma}{dx}}{4\pi R} \sum_{k=1}^{B} \int_0^\infty \frac{[x^2 - xx' \cos \theta_k]x' + [x(\theta \sin \theta_k + \cos \theta_k) - x' \lambda^2}{[x'^2 - 2xx' \cos\theta_k + x^2 + \theta^2\lambda^2]^{3/2}[\lambda^2 + x'^2]^{1/2}} d\theta dx \quad (31)$$

Equation (31) is quite complex and is difficult to handle since the innermost integral contains a singularity at $x = x'$ that is not shown explicitly. This singularity can be made explicit by applying the induction factor, I, introduced by Moriya [22] and defined by equation (22) The induction factor is simply the ratio of the normal induced velocity for a helicoidal trailing vortex system to the normal induced velocity for a straight trailing vortex system of the same strength The induced velocity has a component from the vortex sheet springing from each blade The induced velocity for the helicoidal vortex sheet springing from the blade at which the calculations are being made becomes infinite at $x = x'$ The induced velocity for a straight vortex system also becomes infinite at $x = x'$ The infinite velocity in both cases is a result of that portion of the vortex filament in the neighborhood of the point x'. Since the property of the infinity at $x = x'$ is the same in both cases, the ratio of the two induced velocities must be unity at the point $x = x'$. The contributions to the induction factor at $x = x'$ from all other helicoidal trailing vortices springing from all other blades must be zero since only the blade at which the induced velocity is being calculated has the property of infinity at $x = x'$. Therefore the induction factor takes on the value of unity at $x = x'$.

The induction factor, which is a continuous function of λ, x and x' only, may be evaluated numerically by computer. When x approaches x' the induction factor becomes hard to numerically determine with accuracy. However, since the induction factor is a continuous function and equals unity when $x = x'$, the values when x approaches x' may be interpolated to a high degree of accuracy Typical curves of the induction factor for $\lambda = 0.3$ are shown in Figure 4

The normal induced velocity at a point x' may now be expressed compactly as,

$$w_n(x') = \int_0^1 \frac{\frac{d\Gamma}{dx}}{4\pi R} \frac{I}{x-x'} \, dx \tag{32}$$

The singularity at $x = x'$ is now shown explicitly in equation (32)

The method is now formulated by applying the fundamental equation of finite wing theory,

$$\alpha_g = \alpha_o - \alpha_i \tag{33}$$

α_g is the geometric angle of attack and is defined by

$$\alpha_g = \beta - \text{Arctan} \left(\frac{\lambda}{x'}\right) \tag{34}$$

The effective, or sectional angle of attack, α_o, is evaluated by applying the Kutta-Joukowski theorem and is evaluated as,

$$\alpha_o = \frac{2\,\Gamma}{R\,\Omega\,(\lambda^2 + x'^2)^{1/2}\, a_o \cdot C} \tag{35}$$

The induced angle of attack, α_i is given by

$$\alpha_i = \tan \frac{w_n}{W} \doteq \frac{w_n}{W} \tag{36}$$

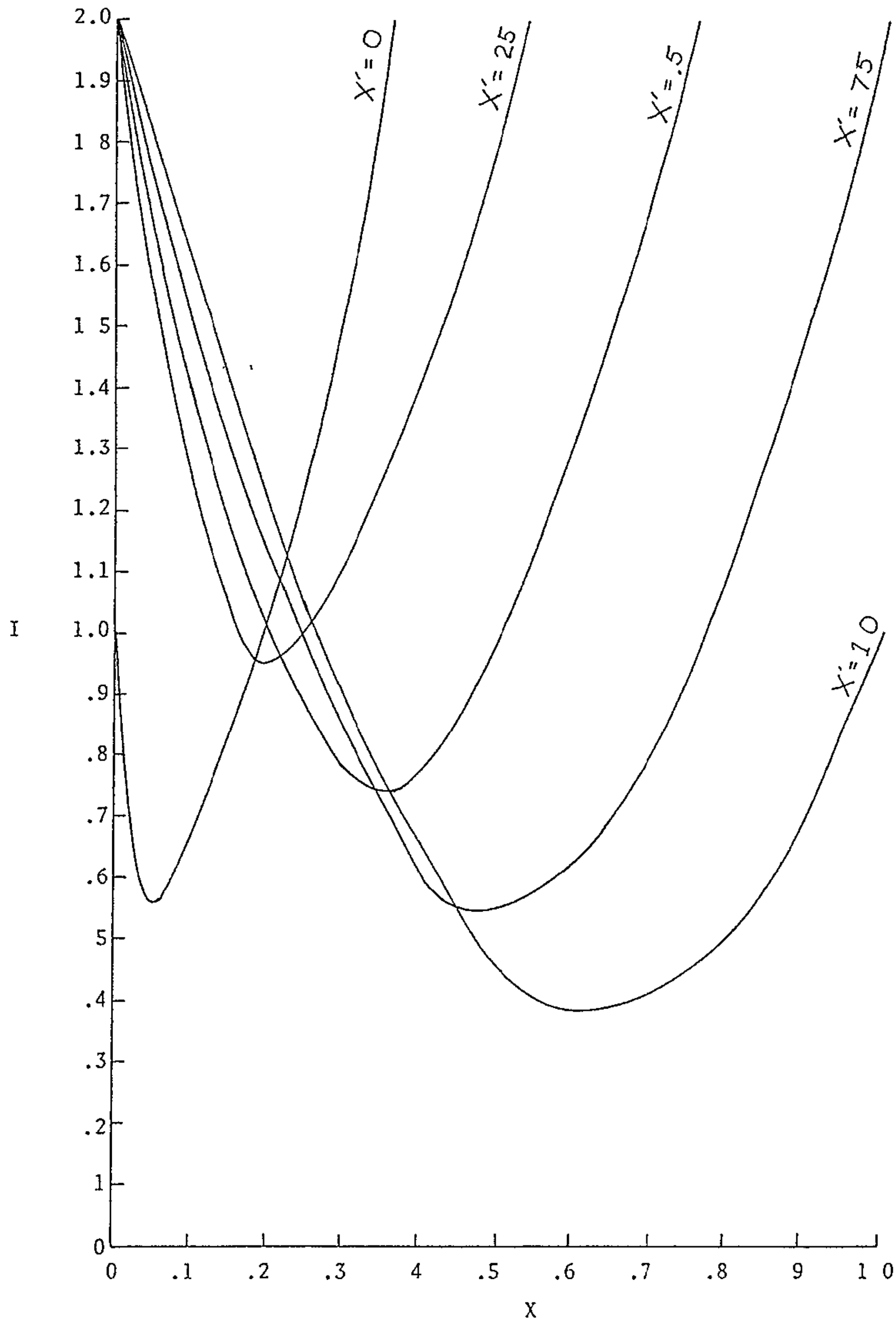

Iigure 4. Induction factor curves for λ = 0 3

Putting equation (34), (35), and (36) into equation (33) results in the fundamental integral equation which must be solved for the circulation, Γ

The boundary condition for the circulation requires that,

$$\Gamma(0) = \Gamma(1) = 0 \tag{37}$$

Therefore, we may express the circulation as a sine series given by

$$\Gamma(x') = \sum_{n=1}^{\infty} A_n \sin n\pi x' \tag{38}$$

Using this series, the fundamental integral equation can be expressed as

$$\frac{2\Sigma A_n \sin n \pi x'}{a_o c R \Omega \ (\lambda^2 + x'^2)^{1/2}} - \frac{\Sigma n \pi A_n}{4\pi R^2\Omega \ (\lambda^2 + x'^2)^{1/2}} \int_0^1 \frac{\cos n \pi x}{x - x'} I dx = \beta - \text{Arctan}\left(\frac{\lambda}{x'}\right) \tag{39}$$

Difficulty now arises in determining the second term in equation (39) since it contains a singularity in the integrand at $x = x'$ This problem is handled by breaking the integral into three separate integrals,

$$\int_0^1 M\,dx = \int_0^{x'-\delta} M\,dx + \int_{x'-\delta}^{x'+\delta} M\,dx + \int_{x'-\delta}^{1} M\,dx \tag{40}$$

where $M = \frac{\cos n\pi x}{x - x'}$ I and δ is a small but finite value The first and third integrals on the right-hand side of equation (40) may be evaluated using established numerical techniques The second term, however, requires special consideration It can be shown that the integrand, M, will go to zero in the limit as δ goes to zero Thus, $\int_{x'-\delta}^{x'+\delta} M\,dx$ will have a finite value.

A method to evaluate this integral for a finite δ is required This is accomplished by first making a variable substitution using,

$$\tau = x - x' \tag{41}$$

The integral can then be written as

$$\int_{-\delta}^{\delta} \frac{\cos n \pi (\tau + x')}{\tau} I \, d\tau \tag{42}$$

Equation (42) is then expanded in a power series in τ. It should be noted that the induction factor, I, is a summation of integrals. The induction factor is a continuous function by virtue of the manner in which it was defined. However, each of the integrals making up the induction factor is not continuous and these integrals do in fact contain singularites. Therefore, it is necessary to expand the induction factor in a power series in a manner which will eliminate these singularities. Since the singularities occur for the helix angle, θ, equal to zero, they may be eliminated by integrating the singular integrals from θ equal ε to ∞ and then separately expanding the integral from θ equal 0 to ε, which contains the singularity. Once the power series in τ is obtained, it is integrated term by term and terms of order τ^2 and larger are dropped. This gives the following approximate relation,

$$\int_{x'-\delta}^{x'+\delta} \frac{\cos n \pi x'}{x - x'} I \, dx = 2\delta \cos (n\pi x') \sum_{k=1}^{2} \int_{\chi'-\delta}^{\chi'+\delta} M \, dx + 2\delta \left[\frac{x' \cos(n\pi x')}{2(\lambda^2 + x'^2)} \right.$$

$$\left. (1 + \ell n(2\varepsilon^2(\lambda^2 + x'^2)) - n\pi \, 2 \sin n\pi x' \right] - \delta \ell n(\delta) \left[\frac{4\lambda' \cos(n\pi x')}{2(x'^2 + \lambda^2)} \right] \tag{43}$$

where ε is a small value and $\varepsilon >> \delta$. The singular integral can thus be approximated for the finite region of width δ around the singularity.

In order to evaluate the coefficients, A_n, of the infinite sine series given in Equation (38), the series is truncated at N terms. The integral Equation (39) is then applied at N locations along the propeller blade. This gives a system of N equations in the N unknowns. This system of equations is solved for the coefficients, A_n, which are used to evaluate the circulation, using Equation (38) The effective angle of attack can then be found using Equation (35). Once the effective angle of attack is found at each designated position along the blade, the lift and drag coefficients can be found directly from the two-dimensional aerodynamic characteristics of the airfoil used at that position on the propeller blade The differential thrust and torque coefficients can be found by applying Equations (2) and (3).

The preceding method has been programmed for use on a digital computer. An explanation of the program is given in Appendix A and a listing of the program is given in Appendix B.

APPENDIX A

Computer Program Explanation

The computer program listed in Appendix B was developed following the method proposed in Section III of this report The variables in Table V must be inputs to the program.

Table V Input Variables to the Computer Program

AO - Lift curve slope per radian.

BT - Blade pitch angle in degrees which must be specified at N locations along the blade.

C - Non-dimensional chord which must be specified at N locations along the blade.

CDO, CD1, CD2 - Drag coefficients of the airfoil section where the total drag coeffieient, $CD = CDO + CD1\ \alpha + CD2\ \alpha^2$.

DEL1 - Interval around the singularity which is not integrated directly.

EL - Tip speed ratio.

N - Number of terms in the sine series

NB - Number of blades.

R - Radius of the propeller in feet.

SKPI1, SKPI2 - The upper and lower limits, respectively, around each of the N blade locations, between which the induction factor is interpolated

WO - Rotational component of tip speed of the propeller in feet per second.

X,W - Languerre-Gauss integration coefficients.

ZTP - N locations along the blade at which the calculations for the sine series are made

The program uses a 44 point Languerre-Gauss integration scheme [25] to do the integration from zero to infinity in order to evaluate the induction factors. Induction factors near x' are interpolated using a spline interpolation formula [26]

$$\int_0^{x'-\delta} M dx \quad \text{and} \quad \int_{x'+\delta}^{1} M dx$$

are found by using a second-order spline integration technique. The spline integration formula is obtained by integrating the spline interpolation formula given in reference [26]. The general form of the spline integration formula for the integral of some function Y between x_1 and x_2 is

$$\int_{x_1}^{x_2} Y\,dx = \frac{C_1}{4}(x_2 - x_1)^4 + \frac{C_2}{4}(x_2 - x_1)^4 + \frac{C_3}{2}(x_2 - x_1)^2 + \frac{C_4}{2}(x_2 - x_1)^2 \tag{45}$$

where the C's are the spline coefficients generated by the spline interpolation routine developed in reference [27]. The spline integration technique has been found to be very accurate since it fits a curve with continuous derivatives through second order to the given function and then integrates the area under this curve. This integration scheme is also used in calculating the total thrust coefficients from the differential thrust coefficients.

A value of δ as small as possible is desired to give the best approximation for $\int_{x'-\delta}^{x'+\delta} M\,dx$.

However, making δ too small causes $\int_0^{x'-\delta} M\,dx$ and $\int_{x'+\delta}^{1} M\,dx$

to become less accurate due to the integrand M becoming very large. A value of δ between 10^{-5} and 10^{-6} has been found to give good results.

The matrix equation for the coefficients of the sine series is solved using Gauss elimination. The answer is checked for accuracy by substituting it back into the matrix equation.

```
C      THIS PROGRAN COMPUTES THE THRUST COEFFICIENT FOR AN ARBITRARY
C      PROPELLER DESIGN USING THE METHOD DEVELOPED IN CHAPTER THREE
C      OF THIS PAPER.
C
C
C      IMPUT VARIABLES TO THE PROGRAM ARE:
C
C      AO - THE LIFT CURVE SLOPE PER RADIAN
C      BT - THE BLADE ANGLE AT EACH OF THE N LOCATIONS ALONG THE BLADE
C      CDO, CD1, CD2 - SECTIONAL DRAG COEFFICIENTS
C      C - THE CHORD NON-DIMENSIONALIZED WITH THE RADIUS
C      DEL1 - THE INTERVAL AROUND THE SINGULARITY THAT IS INTEGRATED
C      SEPARATELY
C      EL - THE TIP SPEED RATIO = V/WO*R
C      EP - A SMALL NUMBER WITH EP>>DEL1
C      N - THE NUMBER OF POINTS IN THE SINE SERIES
C      NB - THE NUMBER OF PROPELLER BLADES
C      R - THE RADIUS OF THE PROPELLER IN FEET
C      SKPI1,SKPI2 - BLADEWISE LOCATIONS BETWEEN WHICH THE INDUCTION
C      FACTOR IS INTERPOLATED
C      WO - THE ROTATIONAL SPEED IN RADIANS/SEC
C      X,W - LANGUERRE-GAUSS INTEGRATION POINTS
C      ZTP - THE N NON-DIMENSIONAL BLADEWISE LOCATIONS AT WHICH
C      THE CALCULATIONS ARE MADE FOR THE SINE SERIES
C
       IMPLICIT REAL*8 (A-H,O-Z)
       INTEGER*4 IDUM(9 )
       DIMENSION ZTP(81), ZT(81), XZ(81), Q(81), AA(4,81),SS(5,81),
     1           QINT(9 ),SINT(9 ),S(81), RINT(9 ),ALPO(9 ),C(9 ),
     2           YI(81), CA(9 ,9 ), RHS(9 ), AS(9 ), CCA(9 ,9 ),
     3           IS(81), TIGRL(11,11), DTC(11), BETA(11)
       COMMON/BBB/X(44), W(44)
       COMMON/CCC/ TT, TTP, PI, EL, EP, NB
C      RADIANS TO DEGREES CONVERSION
       RDC=57.2957795130823D0
       PI=3.14159265358979D0
C      READ IN DATA FOR A 44 POINT LANGUERRE-GAUSS INTEGRATION
       READ(5,5)  (X(L), W(L), L=1,44)
     5 FORMAT (2D30.0)
```

```
      WRITE (6,6)  (X(L), W(L), L=1,44)
    6 FORMAT (' ', D30.15, D30.15)
      N=9
      NB=3
      EL=0.2986D0
      EP=0.30D0
      W0=153.938D0
      A0=0.070D0*RDC
      R=1.40D0
      CD0=0.03334821D0
      CD1=-0.00800893D0*RDC
      CD2=0.00063393D0*RDC**2
C     NP IS THE NUMBER OF POINTS USED IN THE SPLINE INTEGRATION
C     NP MUST BE AT LEAST 4*N SO THAT WHEN INTEGPATING FRON X=0 TO
C     ZTP-DEL OR ZTP+DEL TO 1 THERE WILL ALWAYS BE AT LEAST 4 POINTS
C     FOR THE SPLINE INTEGRATION. (SUBROUTINE SLP1Z WILL FAIL WITH
C     LESS THAN FOUR POINTS)
      NP=(N-1)*10+1
      DO 9 J=1,N
C     READ IN THE BLADE ANGLE, CHORD, AND CORRESPONDING LOCATIONS
C     ON THE BLADE
      READ(5,7) BT, C(J), ZTP(J)
    7 FORMAT (3F10.6)
      BETA(J)=BT/RDC
C     ALPO IS THE GEOMETRIC ANGLE OF ATTACK
      IF (ZTP(J).LE.0.0001D0) ALPO(J)= BT/RDC-PI/2.0D0
      IF (ZTP(J).GT.0.0001D0) ALPO(J)= BT/RDC-DATAN(EL/ZTP(J))
      WRITE (6,8) ZTP(J), BT, ALPO(J), C(J)
    8 FORMAT (' ', 4F20.6)
    9 CONTINUE
      DO 10 I=1,NP
   10 ZT(I)=FLOAT(I-1)/FLOAT(NP-1)
      DEL1=0.000001D0
      DO 400 J=1,N
      DO 4 I=1,NP
      IS(I)=0
    4 YI(I)=0.0D0
      WRITE (6,11) ZTP(J)
   11 FORMAT ('0', 'ZTP=', F8.3)
```

```
      SH=EL**2+ZTP(J)**2
C
C     THIS SECTION CALCULATES ALL THE INDUCTION FACTORS NEEDED
C
      TTP=ZTP(J)
      TT=TTP
      NOPT=2
C     P12 IS THE SUM OF THE INDUCTION FACTORS FOR BLADES 1 AND 2
C     DIVIDED BY (ZT-ZTP)
      CALL CALCI (P12, NOPT)
      NOPT=3
C     P3 IS THE INTEGRAL FROM EP TO INFINITY OF THE INTEGRAND M
C     WHERE I3=(ZT-ZTP)*INTEGRAL OF M
      CALL CALCI(P3, NOPT)
      NOPT=1
      TTP=ZTP(J)
      NAB=0
      NCTR=0
      ICTR=0
C     INTERPOLATE VALUES OF I BETWEEN SKPI1 & SKPI2
C     WHERE SKPI1 & SKPI2 ARE READ IN FOR EACH ZTP LOCATION
      READ(5,12) SKPI1, SKPI2
   12 FORMAT (2F10.3)
      WRITE (6,13) SKPI1, SKPI2
   13 FORMAT ('0','     SKIP DIRECT I CALCULATION BETWEEN ZT=', F7.3,
     1       'AND', F7.3)
      DO 15 I=1,NP
      TT=ZT(I)
C     FIND THE VALUE OF THE DO LOOP PARAMETER FOR WHICH ZT=ZTP
      IF (DABS(TTP-TT).LT.0.000001D0) ICTR=I
      IF (TT.LT.SKPI1.OR.TT.GT.SKPI2) CALL CALCI(XI, NOPT)
C     STORE THE INDUCTION FACTOR IN THE ARRAY YI
      IF (TT.LT.SKPI1.OR.TT.GT.SKPI2) YI(I)=XI
C     STORE WHICH INDUCTION FACTOR  CALCULATIONS HAVE BEEN SKIPPED
      IF (TT.GE.SKPI1.AND.TT.LE.SKPI2) IS(I)=1
   15 CONTINUE
      DO 17 I=1,NP
      ICK=0
      TT=ZT(I)
```

```
      IF (IS(I).NE.1.AND.TT.GE.SKPI1-0.074D0.AND.TT.LE.SKPI2+0.074D0
     1   .OR.I.EQ.ICTR) ICK=2
C     NAB IS THE NUMBER OF POINTS AT WHICH THE DIRECT CALCULATION
C     OF THE INDUCTION FACTOR HAS BEEN CALCULATED
      IF (ICK.EQ.2) NAB=NAB+1
      IF (ICK.EQ.2) XZ(NAB)=TT
C     STORE THE COMPUTED INDUCTION FACTORS IN ARRAY Q
      IF (ICK.EQ.2.AND.I.NE.ICTR) Q(NAB)=YI(I)
      IF (I.EQ.ICTR) Q(NAB)=1.0D0
   17 IF (I.EQ.ICTR) NCTR=NAB
      WRITE (6,21) NAB, ICTR, NCTR
   21 FORMAT  ('0', 'NAB=', 3I10)
      WRITE (6,19) (XZ(L), Q(L), L=1,NAB)
   19 FORMAT (' ', 2F20.5)
C     USE THE SPLINE INTERPOLATION FORMULA TO OBTAIN THE INDUCTION
C     FACTORS THAT WERE SKIPPED IN THE DIRECT CALCULATIONS
C     SLPIZ IS A COMPUTER SUPPLIED SUBROUTINE WHICH WHICH GENERATES
C     SPLINE INTERPOLATION COEFFICIENTS.
      CALL SPL1Z (XZ, Q, NAB, AA, SS)
      DO 18 I=1,NP
      TT=ZT(I)
C     USE SPLINE INTERPOLATION FORMULA
      IF (IS(I).EQ.1.AND.I.LT.ICTR)
     1 YI(I)=AA(1,NCTR-1)*(XZ(NCTR)-TT)**3
     1       +AA(2,NCTR-1)*(TT-XZ(NCTR-1))**3
     2       +AA(3,NCTR-1)*(XZ(NCTR)-TT)
     3       +AA(4,NCTR-1)*(TT-XZ(NCTR-1))
      IF(I.EQ.ICTR) YI(I)=1.0D0
   18 IF (IS(I).EQ.1.AND.I.GT.ICTR)
     1  YI(I)=AA(1,NCTR)*(XZ(NCTR+1)-TT)**3
     2        +AA(2,NCTR)*(TT-XZ(NCTR))**3
     3        +AA(3,NCTR)*(XZ(NCTR+1)-TT)
     4        +AA(4,NCTR)*(TT-XZ(NCTR))
      IF (ZTP(J).GT.DEL1) TT=ZTP(J)-DEL1
      IF (ZTP(J).GT.DEL1)
     1  XIBZ=AA(1,NCTR-1)*(XZ(NCTR)-TT)**3
     1       +AA(2,NCTR-1)*(TT-XZ(NCTR-1))**3
     2       +AA(3,NCTR-1)*(XZ(NCTR)-TT)
     3       +AA(4,NCTR-1)*(TT-XZ(NCTR-1))
```

```
      IF (1.000-ZTP(J).GT.DEL1) TT=ZTP(J)+DEL1
      IF (1.000-ZTP(J).GT.DEL1)
     1   XIAZ=AA(1,NCTR)*(XZ(NCTR+1)-TT)**3
     2        +AA(2,NCTR)*(TT-XZ(NCTR))**3
     3        +AA(3,NCTR)*(XZ(NCTR+1)-TT)
     4        +AA(4,NCTR)*(TT-XZ(NCTR))
C     ALL THE INDUCTION FACTORS HAVE NOW BEEN CALCULATED AND
C     STORED IN YI, XIBZ, XIAZ.  XIBZ & XIAZ ARE THE INDUCTION
C     FACTORS AT ZTP-DEL AND ZTP+DEL RESPECTIVELY.
      DO 210 NS=1,N
      ARG=NS*PI*ZTP(J)
      WRITE (6,20) NS
   20 FORMAT ('0', '+++  NS=', I3, ' +++++++++++')
      DO 22 IJ=1,N
      QINT(IJ)=0.0D0
      RINT(IJ)=0.0D0
   22 SINT(IJ)=0.0D0
      DEL=DEL1
      ND=0
      IF (ZTP(J).LE.DEL) GO TO 53
C
C     THIS SECTION CALULATES THE INTEGRAL FROM 0 TO ZTP-DEL
C
      DO 25 I=1,NP
      ND=ND+1
      IF (ZT(I)-ZTP(J).GE.-DEL1  ) GO TO 30
      XZ(I)=ZT(I)
C     STORE THE INTEGRAND IN ARRAY Q
   25 Q(I)=DCOS(NS*PI*ZT(I))*YI(I)/(ZT(I)-ZTP(J))
   30 XZ(ND)=ZTP(J)-DEL
      Q(ND)=DCOS(NS*PI*XZ(ND))*XIBZ/(XZ(ND)-ZTP(J))
      ND1=ND-1
      IF (NS.EQ.1)            WRITE (6,35) (XZ(L), Q(L), YI(L), L=1,ND1)
      IF (NS.EQ.1)            WRITE (6,35) XZ(ND), Q(ND), XIBZ
   35 FORMAT (' ', 3D15.5)
C     INTEGRATE Q USING SPLINE INTEGRATION FORMULA
      CALL SPL1Z(XZ, Q, ND, AA, SS)
      SUMQ=0.0D0
      ND1=ND-1
```

```
      DO 40 K=1,ND1
   40 SUMQ=SUMQ+.25DO*AA(1,K)*(XZ(K+1)-XZ(K))**4
     1          +.25DO*AA(2,K)*(XZ(K+1)-XZ(K))**4
     2          +.50DO*AA(3,K)*(XZ(K+1)-XZ(K))**2
     3          +.50DO*AA(4,K)*(XZ(K+1)-XZ(K))**2
      QINT(NS)=SUMQ
      WRITE (6,50) SUMQ
   50 FORMAT (' ', 'INTEGRAL OF Q=', E11.3)
   53 CONTINUE
      IF (IGT.EQ.1) GO TO 75
      IF (ZTP(J).LT.DEL.OR.1.0DO-ZTP(J).LT.DEL) DEL=DEL/2.0DO
C
C     THIS SECTION CALULATES THE INTEGRAL FROM ZTP-DEL TO ZTP+DEL
C
      ATERM=DCOS(ARG)*2.0DO*DEL*P12
      BTERM1=2.0DO*DEL*((ZTP(J)*DCOS(ARG))/(DSQRT(2.0DO)*SH)
     1                 *(1.0DO+DLOG(2.0DO*EP**2*SH))
     2                 -NS*PI*DSQRT(2.0DO)*DSIN(ARG))
      BTERM2= -DEL* DLOG(DEL1)*(4.0DO*ZTP(J)*DCOS(ARG)
     1                          /(DSQRT(2.0DO)*SH))
      CTERM=2.0DO*DCOS(ARG)*DEL*P3
      RINT(NS)=ATERM+BTERM1+BTERM2+CTERM
      IF (NS.EQ.1) WRITE (6,55) P12, P3
   55 FORMAT ('0', 2E20.5)
      IF (NS.EQ.1) WRITE (6,60) ATERM, BTERM1, BTERM2, CTERM
   60 FORMAT ('0', 4E20.5)
      WRITE (6,70) RINT(NS)
   70 FORMAT (' ', 'INTEGRAL OF R=', E11.3)
      DEL=DEL1
   75 RINT(NS)=0.0DO
      IF (1.0DO-ZTP(J).LE.DEL) GO TO 160
C
C     THIS SECTION CALULATES THE INTEGRAL FROM ZTP+DEL TO 1.0
C
      ND=1
      XZ(ND)=ZTP(J)+DEL
      S(ND)=DCOS(NS*PI*XZ(ND))*XIAZ/(XZ(ND)-ZTP(J))
      DO 100 I=1,NP
      IF (ZT(I)-ZTP(J).LE.DEL1   ) GO TO 100
```

```
      ND=ND+1
      XZ(ND)=ZT(I)
C     STORE THE INEGRAND IN ARRAY S
      S(ND)=DCOS(NS*PI*ZT(I))*YI(I)/(ZT(I)-ZTP(J))
  100 CONTINUE
  110 CONTINUE
      IF (NS.EQ.1)           WRITE (6,35) XZ(1), S(1), XIAZ
      LND=NP-ND
      DO 115 L=2,ND
      LL=L+LND
      IF (NS.EQ.1)           WRITE (6,35) XZ(L), S(L), YI(LL)
  115 CONTINUE
C     INTGRATE S USING SPLINE INTEGRATION FORMULA
      CALL SPL1Z(XZ, S, ND, AA, SS)
      SUMS=0.0D0
      ND1=ND-1
      DO 140 K=1,ND1
  140 SUMS=SUMS+.25D0*AA(1,K)*(XZ(K+1)-XZ(K))**4
     1          +.25D0*AA(2,K)*(XZ(K+1)-XZ(K))**4
     2          +.50D0*AA(3,K)*(XZ(K+1)-XZ(K))**2
     3          +.50D0*AA(4,K)*(XZ(K+1)-XZ(K))**2
      SINT(NS)=SUMS
      WRITE(6,150) SUMS
  150 FORMAT (' ', 'INTEGRAL OF S=', E12.4)
C     TINT IS THE TOTAL INTEGRAL FROM ZERO TO 1
  160 TINT=QINT(NS)+RINT(NS)+SINT(NS)
      TIGRL(J,NS)=TINT
      WRITE(6,170) TINT
  170 FORMAT ('0', 'TOTAL INTEGRAL FROM 0 TO INFINITY=', E20.5)
C     SET UP THE MATRIX EQUATION
      CA(J,NS)=2.0D0*DSIN(NS*PI*ZTP(J))/A0-NS*C(J)*TINT/(4.0D0*2)
      CCA(J,NS)=CA(J,NS)
  210 CONTINUE
      RHS(J)=W0*R[illegible]*DSQRT(SH)*ALPO(J)*C(J)
      WRITE (6,350)
  350 FORMAT ('0', '***************************************************
     1********************************')
  400 CONTINUE
      WRITE(6,500) ((CA(M,L), L=1,N), M=1,N)
```

```
  500 FORMAT (' ',  9F11.5)
      WRITE (6,550) (RHS(L), L=1,N)
  550 FORMAT ('0',  9F11.3)
C     SOLVE THE MATRIX EQUATION FOR THE AS VALUES USING A
C     COMPUTER SUPPLIED GAUSS ELIMINATION TECHNIQUE.
      CALL GAUSZ (CA, N, N, RHS, AS, IDUM, IER)
      WRITE (6,600) (AS(L), L=1,N)
  600 FORMAT (' ', 'A=', D20.5)
      WRITE (6,625)
  625 FORMAT ('0', 11X, 'ZETA', 16X, 'GAMA', 16X, 'ALPHA I',
     1           14X, 'ALPHA O', 14X, 'DTC', 14X, 'PHI')
      DO 700 NK=1,N
      STIGR=0.0D0
      SGAM=0.0D0
      VC=WO*R**2*DSQRT(EL**2+ZTP(NK)**2)
C     VR IS THE RELATIVE VELOCITY
      VR=VC/R
      DO 650 K=1,N
      STIGR=STIGR+TIGRL(NK,K)*AS(K)*K
C     CALULATE THE CIRCULATION
  650 SGAM=SGAM+AS(K)*DSIN(K*PI*ZTP(NK))
      ALI=STIGR/(4.0D0*VR)
C     CALCULATE THE EFFECTIVE ANGLE OF ATTACK
      ALO=2.0D0*SGAM/(A0*C(NK)*VC)
      PHI=BETA(NK)-ALO
      IF (ALO.LE.0.108D0) CL=0.11D0*RDC*ALO
C     CALCULATE THE LIFT COEFFICIENT
      IF (ALO.GT.0.108D0) CL=0.070D0*RDC*(ALO-0.108D0)+0.7D0
C     CALCULATE THE DRAG COEFFICIENT
      CD=CD0+CD1*ALO*CD2*ALO**2
      CY=CL*DCOS(PHI)-CD*DSIN(PHI)
C     CALCULATE THE DIFFERENTIAL THRUST
      DTC(NK)= NB*C(NK)*VR**2*CY/(2.0D0*PI*R**2*WO**2)*(0.25D0*PI**3)
      WRITE(6,675) ZTP(NK), SGAM, ALI, ALO, DTC(NK), PHI
  675 FORMAT (' ', 6E20.5)
  700 CONTINUE
C     INTEGRATE THE THRUST OVER THE BLADE USING SPLINE INTEGRATION
C     FORMULA
      CALL SPL1Z(ZTP, DTC, N, AA, SS)
```

```
      NM1=N-1
      SUMT=0.0D0
      DO 702 K=1,NM1
  702 SUMT=SUMT+.250D0*AA(2,K)*(ZTP(K+1)-ZTP(K))**4
     1           +.500D0*AA(4,K)*(ZTP(K+1)-ZTP(K))**2
     2           +.250D0*AA(1,K)*(ZTP(K+1)-ZTP(K))**4
     3           +.500D0*AA(3,K)*(ZTP(K+1)-ZTP(K))**2
      WRITE (6,705) SUMT
  705 FORMAT ('0', 'THRUST COEFFICIENT=', F20.7)
C     CHECK TO SEE IF THE MATRIX EQUATION WAS SOLVED CORRECTLY
      DO 725 I=1,N
      CKRHS=0.0
      DO 710 J=1,N
  710 CKRHS=CCA(I,J)*AS(J)+CKRHS
  725 WRITE (6,730) CKRHS
  730 FORMAT ('0', F20.3)
      RETURN
      END
C
C
      SUBROUTINE CALCI (XI, NOPT)
C     THIS SUBROUTINE CALCULATES THE INDUCTION FACTORS AS FOLLOWS:
C     NOPT = 1  CALCULATES I1+I2+I3=I
C     NOPT = 2  CALULATES THE INTEGRAL OF P1+P2 FROM 0 TO INFINITY
C     NOPT = 3  CALULATES THE INTEGRAL OF P3 FROM EPSILON TO INFINITY
C     WHERE I=(ZT-ZTP)*(P1+P2+P3)
      IMPLICIT REAL*8 (A-H,O-Z)
      COMMON/AAA/ KK, NNOPT
      COMMON/CCC/ TT, TTP, PI, EL, EP, NB
      DIMENSION AN(3)
      EXTERNAL AUX
      NNOPT=NOPT
      DO 10 KK=1,3
      IF (NOPT.EQ.2.AND.KK.EQ.3) GO TO 20
      IF (NOPT .EQ.3.AND.KK.NE.3) GO TO 10
      CALL GLQU (AUX, ANS)
   10 AN(KK)=ANS
      IF (NOPT.EQ.1.AND.DABS(TT-TTP).LE.0.001D0)
     1                XI=1.0D0
```

```
      IF (NOPT.EQ.1.AND.DABS(TT-TTP).GT.0.001D0)
     1               XI=(AN(1)+AN(2)+AN(3))*(TT-TTP)
   20 IF (NOPT.EQ.2) XI=AN(1)+AN(2)
      IF (NOPT.EQ.3) XI=AN(3)
      RETURN
      END
C
C
      SUBROUTINE GLQU (AUX,ANS)
C     THIS SUBROUTINE SETS UP THE LANGUERRE-GAUSS INTEGRATION
      IMPLICIT REAL*8 (A-H,O-Z)
      COMMON/BBB/X(44), W(44)
  200 ANS=0.0D0
      S=0.0D0
      DO 201 I=1,44
      Y=X(I)
      CALL AUX(Y,Z)
  201 S=S+Z*W(I)
      ANS=S
      RETURN
      END
C
C
      SUBROUTINE AUX (PHI, FX)
C     THIS SUBROUTINE CALCULATES THE INTEGRAND OF P1, P2, & P3
C     WHERE THE INDUCTION FACTOR = (ZT-ZTP)*INTGRAL OF (P1, P2, &P3)
C     NOTE THAT THE INTEGRAND OF P IS GIVEN BY A/B BELOW
      IMPLICIT REAL*8 (A-H,O-Z)
      COMMON/CCC/ TT, TTP, PI, EL, EP, NB
      COMMON/AAA/ KK, NOPT
      IF (NOPT.EQ.3) PHI=PHI+EP
(TT*TTP)
      PHIK=PHI+2.0D0*PI*(NB-KK)/NB
      A=(TT**2)*(TT-TTP*DCOS(PHIK))+(TT*(PHI*DSIN(PHIK)+DCOS(PHIK))-TTP)
     1  *EL**2
      B=(DSQRT(TT**2+TTP**2-2.0D0*TT*TTP*DCOS(PHIK)+PHI**2*EL**2))**3
     1   *DSQRT(EL**2+TT**2)
                  TTP
      C=A/B
      FX=DEXP(PHI)*C
      RETURN
```

REFERENCES

1. Froude, W , "On the elementary relation between pitch, slip and propulsive efficiency," Transaction of the Institute of Naval Architects, Vol. 19, 1878.

2. Rankine, W. J M , "On the mechanical principles of the action of propellers," Transaction of the Institute of Naval architects, Vol. 6, 1865

3. Dommasch, D. O., "Elements of Propeller and Helicopter Aerodynamics," Pitman, New York, 1953.

4. McCormick, B. W., "Aerodynamics of V/STOL Flight," Academic Press, New York, 1967.

5. Durrand, W F., "Aerodynamic Theory, Vol IV," Julius Springer, Berlin, 1945

6. Glauert, H., "The Elements of Aerofoil and Airscrew Theory," University Press, Cambridge, 1948

7. Glauert, H , "An Aerodynamic Theory of the Airscrew," Aeronautical Research Committee Reports and Memoranda No. 786, 1922

8. Glauert, H , and Lock, C N. H , "The Accuracy of the Vortex Theory of Airscrews in the Light of Recent Experimental Work and Its Application to Airscrew Design," Aeronautical Research Committee Reports and Memoranda No 1040, 1926.

9. Goldstein, S , "On the vortex theory of screw propellers," Proceedings of the Royal Society of London, Series A, Vol. 123, 1929

10. Lock, C N H , "Application of Goldstein\s Airscrew Theory to Design," Aeronautical Research Committee Reports and Memoranda No 1377, 1930

11 Theodorsen, T , "Theory of Propellers," McGraw-Hill, New York, 1948.

12. Theodorsen, T , "The Theory of Propellers I - Determination of the Circulation Function and Mass Coefficient for Dual-Rotating Propellers," NACA Report 775, 1944.

13. Theodorsen, T , "The Theory of Propellers II - Method for Calculating the Axial Interference Velocity," NACA Report 776, 1944.

14. Theodorsen, T., "The Theory of Propellers III - The Slipstream Contraction with Numerical Vlues for Two-Blade and Four-Blade Propellers," NACA Report 777, 1944

15. Theodorsen, T , "The Theory of Propellers IV - Thrust Energy and Efficiency Formulas for Single and Dual-Rotating Propellers with Ideal Circulation Distribution," NACA Report 778, 1944.

16. Crigher, J , "Application of Theodorsen's Theory to Propeller Design," NACA Report 924, 1949.

17. Lock, C. N. H , "Application of Prandtl Theory to an Airscrew," Aeronautical Research Committee Reports and Memoranda No. 1521, 1932.

18. Lock, C. N H , "Airscrew Theory," Aeronautical Research Committee Reports and Memoranda No. 1746, 1936.

19. Lock, C N. H. and Yeatman, D., "Tables for use in an Improved Method of Airscrew Strip Theory Calculation," Aeronautical Research Committee Reports and Memoranda No. 1674, 1934.

20. Lock, C. N H., "A Graphical Method of Calculating the Performance of an Airscrew," Aeronautical Research Committee Report and Memoranda No. 1849, 1937.

21. Prandtl, L , "Application of Modern Hydrodynamics to Aeronautics," NACA Report 116, 1921.

22. Moriya, T., "Selected Scientific and Technical Papers," University of Tokyo, Tokyo, 1959

23 Reid, E , "The Influence of Blade-Width Distribution on Propeller Characteristics," NACA Technical Note 1834, 1949

24. Stack, J , "Test of Airfoils Designed to Delay the Compressibility Burble," NACA Report 763, 1943

25. Stoud, A. and Secrest, D , "Gaussian Quadrature Formulas," Prentice-Hall, Englewood Cliffs, New Jersey, 1966.

26. Pennington, R. H , "Introductory Computer Methods and Numerical Analysis," MacMillan Company, London, 1970

27. FORTUOI Writeups, Computing Services Offices, University of Illinois, Urbana, 1974.

APPENDIX B

FORMER APPROACH TO THE PROPELLER NOISE PROBLEM

by C. J Woan

LIST OF MAIN SYMBOLS

a_o speed of sound

I acoustic intensity

$\ell(r)$ thrust per unit length

$\overline{M} = \overline{V}/a_o$

$\overline{M}_f = \overline{V}_f/a_o$

$M_t = r_t\Omega/a_o$

$M_R = \overline{M}\cdot\overline{R}/R$

p' acoustic pressure

p'_t acoustic pressure due to thrust

$\overline{R} = \overline{X} - \overline{Y}$

r_t radius of propeller

T total thrust

t observation time

$\overline{V}$ the velocity of source

$\overline{V}_f$ forward velocity of propeller

$\overline{X}$ field point

$x_o = (x_{01}^2 + x_{02}^2 + x_{03}^2)^{1/2}$ the distance between the field point and the center of the propeller at t

$\overline{Y}$ source point

θ the instantaneous angle the source makes with y_2 - axis

θ_o initial angular displacement

Ψ $\tan\Psi = x_{02}/x_{01}$

τ retarded time

Ω angular velocity of propeller

$[f(t)] \equiv f(\tau)$

B-2

1. Coordinate System and Geometry

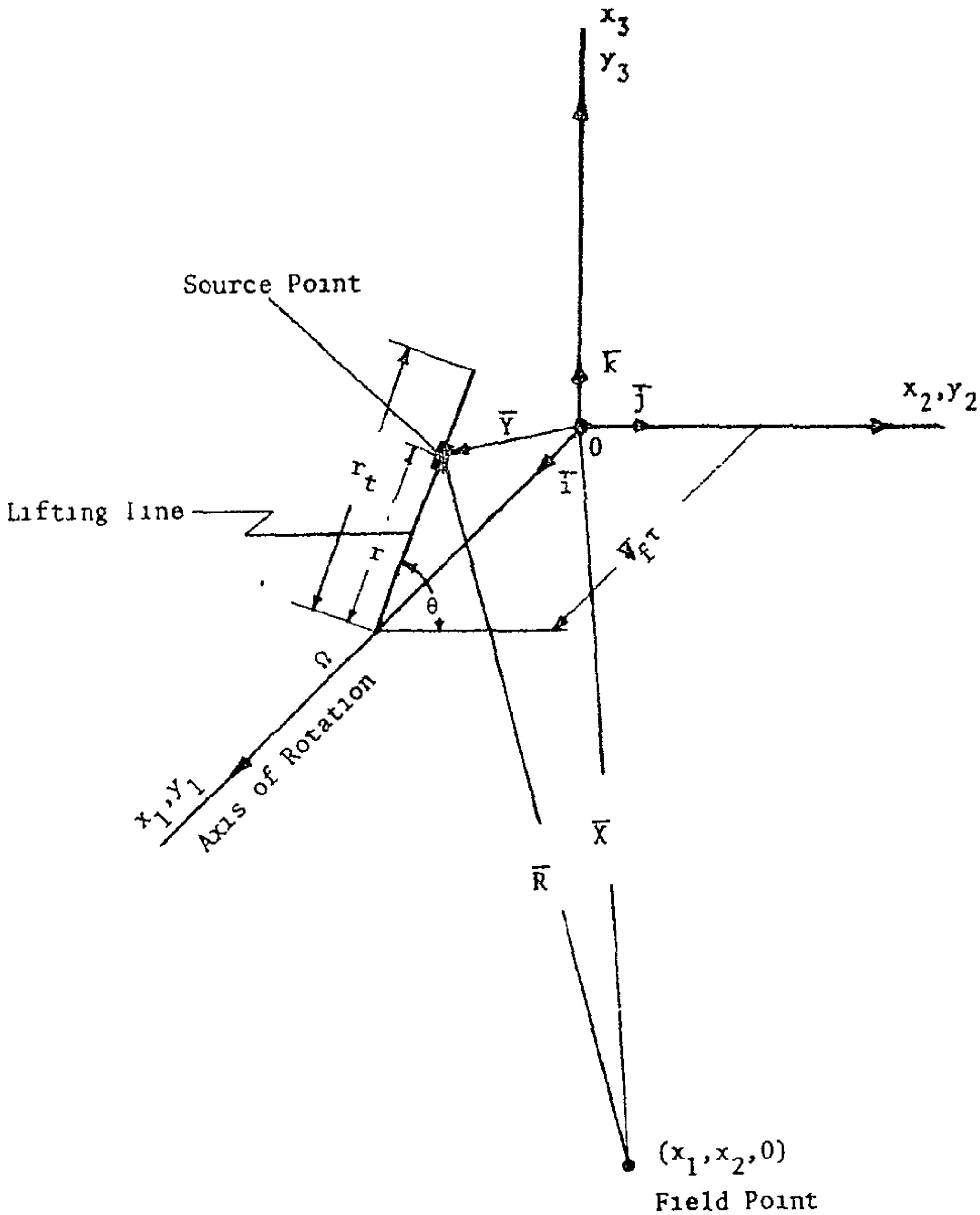

Figure 1 Coordinate System

2. Acoustic Pressure Perturbation

Following Ffowcs Williams and Hawkings, the acoustic pressure perturbation at the field point is given by

$$P' = -\frac{1}{4\pi}\frac{\partial}{\partial x_i}\int\left[\frac{P_i}{R|1-M_R|}\right]dS$$

where dS is the blade surface area and P_i is the i^{th} component of the force acting on air by the blade surface

3 Noise Due To Thrust

Let $\ell(r)$ be the spanwise distribution of the thrust along the lifting line per unit length Then

$$P' = -\frac{1}{4\pi}\frac{\partial}{\partial x_i}\int_0^{r_t}\left(\left[\frac{x_i - y_i}{a_0 R^2(1-M_R)^2}\left\{\frac{\partial P_i}{\partial t} + \frac{P_i}{1-M_R}\frac{\bar{R}}{R}\cdot\frac{\partial\bar{M}}{\partial t}\right\}\right]\right.$$

$$\left. + \left[\frac{1}{R^2(1-M_R)^2}\left\{\frac{P_i(x_i - y_i)}{R}\frac{1-M^2}{1-M_R} - P_i M_i\right\}\right]\right) dr$$

where $P_1 = -\ell(r)$

$P_2 = 0$

$P_3 = 0$

Therefore the pressure perturbation due to thrust is

$$P_t' = \frac{T}{4\pi r_t^2}\int_0^1 f_t(r^*, \theta_0)\,\bar{\ell}^*(r^*)\,dr^*$$

where

$$r^* = \frac{r}{r_t}, \quad \lambda = \frac{a_0}{\Omega}, \quad R^* = \frac{R}{\lambda}$$

$$t^* = \Omega t, \quad \tau^* = \Omega\tau, \quad x_0^* = \frac{x_0}{\lambda}$$

$$\bar{\ell}(r^*) = \frac{\ell(r)}{\left(\frac{T}{r_t}\right)} = \bar{\ell}^*(r^*)\, r^*\,(1-r^*)$$

T is the total thrust

and

$$f_t(r^*, \theta_o) = M_t^2\, r^*(1-r^*)\Big\{ r^* M_t\, x_o^{*2} \sin\psi \cos\psi \frac{\cos[\theta]}{[R^*]^3[1-M_R]^3}$$

$$+ r^* M_t\, x_o^* \sin\psi \frac{\cos[\theta]}{[R^*]^2[1-M_R]^3} + r^* M_t\, x_o^* M_f \sin\psi \frac{\sin[\theta]}{[R^*]^3[1-M_R]^3}$$

$$- x_o^* \cos\psi \frac{1}{[R^*]^3[1-M_R]^3}\Big\}$$

where the angle θ_o is uniformly distributed over $(0,2\pi)$ Then the probability density function for the random variable θ_o is

$$p(\theta_o) = \frac{1}{2\pi} \qquad 0 \leq \theta \leq 2\pi$$

$$= 0 \qquad \text{otherwise}$$

Therefore, the mean square of P_t' is

$$E(P_t'^2) = \int P_t'^2\, p(\theta_o)\, d\theta_o = \frac{1}{2\pi}\int_0^{2\pi} P_t'^2\, d\theta_o$$

The intensity

$$I = \frac{E(P_t'^2)}{\rho_o a_o}$$

Then define

$$I^* = \frac{I}{\frac{T^2}{r_t^4 \rho_o a_o}} = \int_0^1\!\!\int_0^1 F(r^*, r_1^*)\, \bar{\ell}^*(r^*)\, \bar{\ell}(r_1^*)\, dr^* dr_1^*$$

where

$$F(r^*, r_1^*) = \frac{1}{32\pi^3} \int_0^{2\pi} f_t(r^*, \theta_o)\, f_t(r_1^*, \theta_o)\, d\theta_o$$

The total thrust is given by

$$T = T \int_0^1 \bar{\ell}^*(r^*)\, r^*(1-r^*)\, dr^*$$

Letting

$$J = 1 = \int_0^1 \bar{\ell}^*(r^*)\, r^*(1-r^*)\, dr^* \tag{1}$$

the necessary condition that I* be an extremum, subject to the constraint J = const (i.e. constant total thrust) is

$$\int_0^1 F(r^*, r_1^*)\, \bar{\ell}^*(r_1^*)\, dr_1^* = -\frac{b}{2}\, r^*(1-r^*) \tag{2}$$

where b is a Lagrangian multiplier

and $\bar{\ell}^*(r^*)$ and b can be obtained by solving equations (1) and (2)

4. Numerical Method

The equations needed to solve this problem are

(A) $$\int_0^1 \bar{\ell}^*(r^*)\, r^*(1-r^*)\, dr^* = 1$$

(B) $$\int_0^1 F(r^*, r_1^*)\, \bar{\ell}^*(r_1^*)\, dr_1^* = -\frac{b}{2}\, r^*(1-r^*)$$

(C) $$F(r^*, r_1^*) = \frac{1}{32\pi^3} \int_0^{2\pi} f_t(r^*, \theta_o)\, f_t(r_1^*, \theta_o)\, d\theta_o$$

(D) $$f_t(r^*, \theta_o) = M_t^2 r^*(1-r^*) \Big\{ r^* M_t x_o^{*2} \sin\psi \cos\psi \frac{\cos[\theta]}{[R^*]^3[1-M_R]^3} + r^* M_t x_o^* \sin\psi \frac{\cos[\theta]}{R^{*2}[1-M_R]^3} + r^* M_t x_o^* \sin\psi \frac{\sin[\theta]}{[R^*]^3[1-M_R]^3} - \frac{x_o^* \cos\psi}{[R_o^*]^3[1-M_R]^3}$$

(E). $$[R^*] = \left\{ \left(x_0^* \cos\psi + M_f [R^*] \right)^2 + x_0^{*2} \sin^2\psi + r^{*2} M_t^2 - 2 x_0^* r^* M_t \sin\psi \cos(\theta_0 + t^* - [R^*]) \right\}^{1/2}$$

(F) $$[\theta] = \theta_0 + t^* - [R^*]$$

(G). $$[1 - M_R] = (1 - M_f^2) - \frac{x_0^*}{[R^*]} \left(M_f \cos\psi - r^* M_t \sin\psi \sin[\theta] \right)$$

The solution proceeds as follows

Given M_F, M_T, x_o^*, and Ψ, find b and $\overline{\ell}^*(r^*)$

1 The integrals in equations (A), (B), and (C) are calculated by Gaussian integration (Gauss-Legendre formulas or Gauss-Chebyshev formulas).

2 Equation (E) is solved by the Newton Method

$$[R^*]_n = [R^*]_{n-1} - \frac{f([R^*]_{n-1})}{f'([R^*]_{n-1})}$$

$$f([R^*]) = [R^*] - \left\{ \left(x_0^* \cos\psi + M_f [R^*] \right)^2 + x_0^{*2} \sin^2\psi + r^{*2} M_t^2 - 2 x_0^* r^* M_t \sin\psi \cos(\theta_0 + t^* - [R]) \right\}^{\frac{1}{2}}$$

3 After obtaining $[R^*]$ from (2), the value of $[R^*]$ is substituted into equations (A), (B), (C), (D), (F), and (G)

4. After applying Gaussian integration to equation (B) and assigning n different values for r^* ($o \leq r \leq 1$, n = the number of points used in Gaussian integration), equation (B) can be reduced to a system of n equations with unknowns $\overline{\ell}^*(r_i^*)$ ($i=1,2,--,n$) [r_i^* are the zeros of the n^{th} polynomial used in the Gaussian integration]

In matrix form

$AL = C$

A. nxn matrix

C: column matrix

$L = (\bar{\ell}^*(r_1^*), \bar{\ell}^*(r_2^*), \cdots, \bar{\ell}^*(r_n^*))^T$

5 The Lagrangian multiplier is obtained by substituting $\bar{\ell}^*(r_1^*)$ obtained from (4) into equation (A).

APPENDIX C

PRESENT APPROACH TO THE PROPELLER NOISE PROBLEM

by C. J. Woan

LIST OF SYMBOLS

A_i	Fourier coefficients of Γ
a_o	speed of sound
B	number of propeller blades
C_m	complex magnitude of the m^{th} harmonic
dD	drag per unit length
dL	lift per unit length
I	acoustic intensity
$J_{m(Z)}$	Bessel function of order m and argument Z
$\overline{M}$	$= \overline{V}/a_o$
M_R	$= \overline{M} \cdot \overline{R}/R$
$P-P_o$	acoustic pressure
P_{rms}	root-mean-square pressure
$\overline{R}$	$= \overline{X} - \overline{Y}$
R_o	$= x^2+y^2+z^2$
r_t	radius of propeller
T_t	total thrust
t	observation time
$\overline{V}$	the velocity of source
$\overline{V}_F$	forward velocity of propeller
W_i	induced velocity
$\overline{X}$	field point
$\overline{Y}$	source point
α_i	induced angle of attack
ϕ	initial angular displacement
θ	the instantaneous angle the source makes with the y_2 - axis
ρ_o	fluid density
Γ	spanwise circulation distribution
τ	retarded time
Ω	angular velocity of propeller

$[f(t)] \equiv f(\tau)$

1. Coordinate System and Geometry

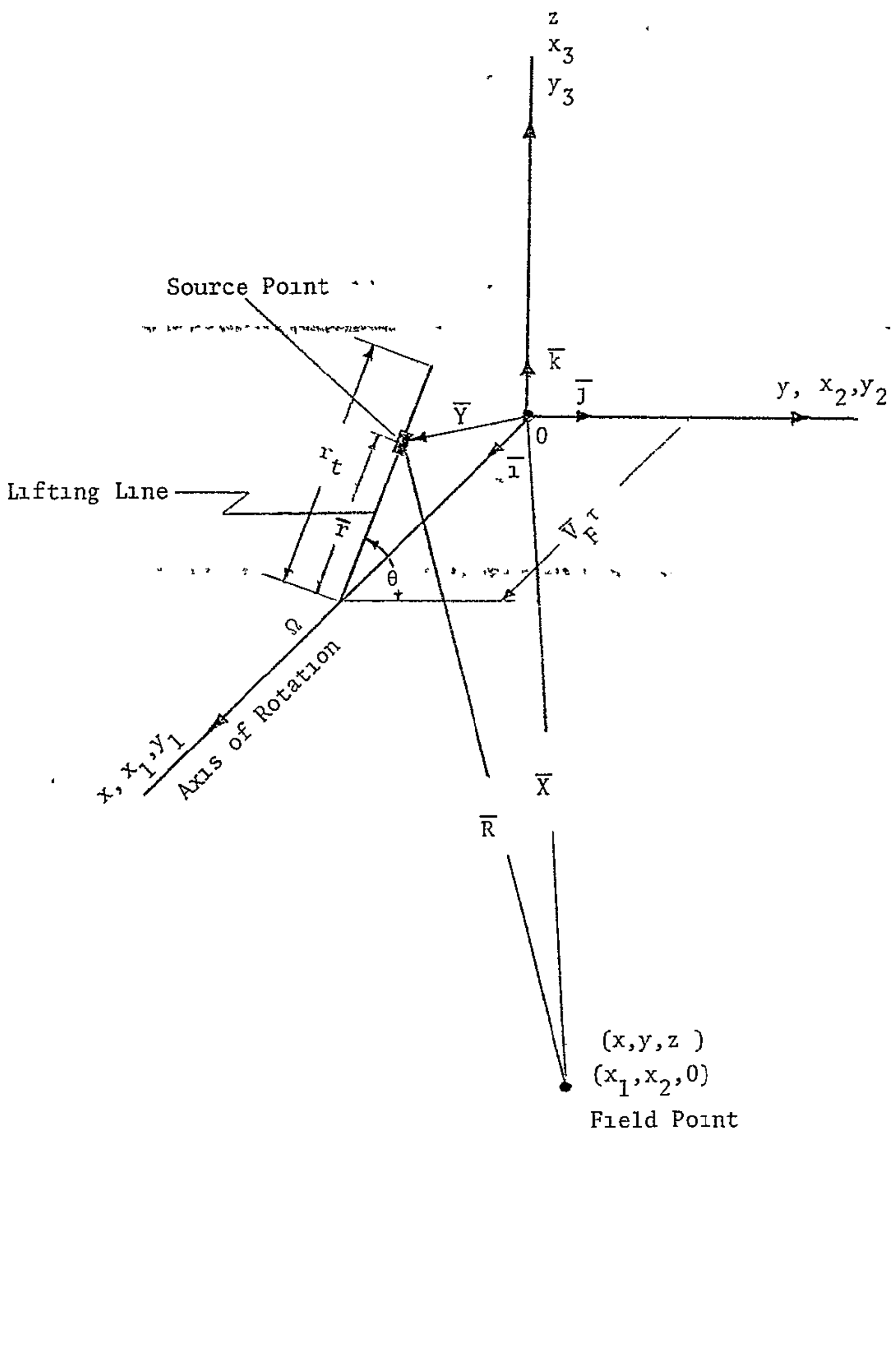

Figure 1 Coordinate System

2. Sound Pressure Due to Moving Lifting Line

The force acting on the air at $\overline{Y} = \Omega\tau + \overline{r}$, by the moving lifting line, is developed as follows

Consider a blade element at location r

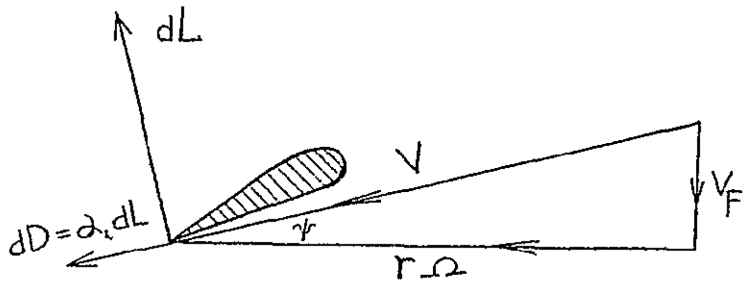

$$dF_x = -(dL\cos\psi - dD\sin\psi)\ , \quad dF_\theta = dL\sin\psi + dD\cos\psi$$

The force, $d\overline{F}$, acting on the air at $\overline{Y} = \Omega\tau + \overline{r}$ is

$$d\overline{F} = dF_x\ \overline{i} - dF_\theta \sin\theta\ \overline{j} + dF_\theta \cos\theta\ \overline{k}$$

The total sound pressure generated by the moving lifting line is given as

$$(P - P_0)(\overline{x}, t) = -\frac{1}{4\pi}\frac{\partial}{\partial x_i}\int \left[\frac{dF_i}{R(1 - M_R)}\right]$$

3 Periodicity of the Acoustic Pressure Disturbance

Consider a propeller whose hub is moving with constant velocity $\overline{V}_F$

Choose fixed axes O_{xyz} such that the origin coincides with the hub

(i) at time $\tau = 0$

(ii) the x axis is parallel to the axis of rotation

(iii) the hub velocity vector lies in the plane and in x-direction.

Let the field point $\overline{X}$ be at (x,y,z) and a typical source point be situated at $\overline{Y}(t)$ This can be expressed as the vector sum of the hub location and the rotational position

$$\overline{Y}(\tau) = \overline{V}_F \tau + \overline{r}(\tau), \qquad \overline{r}(\tau) = (0, r\cos\theta, r\sin\theta).$$

Here θ is the instantaneous angle the source makes with y axis This increases linearly with time, and can be expressed as $\Omega\tau+\phi$ where Ω is the angular velocity of the source, and ϕ is the initial angular displacement.

$$\tau = t - \frac{[R]}{a_o}$$

If attention is confined to source times near τ=0, [R] can be approximated by

$$[R] = \left\{ (x - V_F)^2 + (y - r\cos[\theta])^2 + (z - r\sin[\theta])^2 \right\}^{1/2}$$

$$= R_o (1 + \varepsilon)^{1/2}$$

where $R_o = (x^2 + y^2 + z^2)^{1/2}$

and

$$\varepsilon = \left\{ r^2 - 2r(y\cos[\theta] + z\sin[\theta] + V_F^2\tau^2 - 2xV_F\tau \right\} / R_o^2$$

Therefore,

$$[R] \doteq R_o - \frac{x}{R_o} V_F \tau - \frac{r}{R_o}(y\cos[\theta] + z\sin[0])$$

and

$$\Omega t - \Omega \frac{R_o}{a_o} = \Omega\tau(1 - M_{or}) - M_r(y\cos[\theta] + z\sin[\theta])$$

where

$$M_{or} = \frac{x V_F}{a_o R_o} \qquad \text{and} \qquad M_r = \frac{\Omega r}{a_o}$$

This equation shows that as θ increases by 2π, Ωt only increases by $2\pi(1-M_{or})$. Hence the basic observed frequency is $\omega=\Omega/(1-M_{or})$ and therefore $P-P_o$ has a period $2\pi/\omega$

4 Fourier Analysis

$(P-P_o)(\overline{X},t)$ has a period $\frac{2\pi}{\omega}$, where $\omega = \Omega/(r-M_{or})$ and $M_{or} = \frac{V_F x}{R_o a_o}$

Then, defining the complex matnitude of the m^{th} harmonic in the usual way

$$C_m(\overline{X}) = a_m + i\, b_m = \frac{\omega}{\pi}\int_0^{\frac{2\pi}{\omega}} (P-P_o)(\overline{X},t)\, e^{im\omega t}\, dt$$

$$= -\frac{1}{4\pi}\int \frac{\partial}{\partial x_i} I_i$$

where $$I_i = \frac{\omega}{\pi}\int \left[\frac{dF_i}{R(1-M_R)}\right] e^{im\omega t}\, dt$$

changing variables back to the retarded time, τ, gives

$$I_i = \frac{\omega}{\pi}\int \left[\frac{dF_i}{R}\right] e^{im\omega(\tau + \frac{[R]}{a_o})}\, d\tau$$

where $dt = [1-M_R]\, d\tau$

$$[R] \doteq R_o - a_o M_{or}\tau - \frac{r}{R_o}(y\cos[\theta] + z\sin[\theta])$$

Since the far field approximation is in force, the only significant dependence of F_i upon x_i is through the R_o term in the exponent.

Therefore

$$\frac{\partial I_i}{\partial x_i} = \frac{i m \omega^2}{a_o \pi} \int \left[dF_i \cdot \frac{\partial R_o}{\partial x_i} \right] e^{i m \omega \left(\tau + \frac{[R]}{a_o} \right)} \quad \frac{d\tau}{R_o}$$

and

$$C_m = \frac{-i m \omega e^{i m \omega \frac{R_o}{a_o} - i m \phi}}{2 \pi a_o R_o (1 - M_{or})} (-i)^m \int J_m \left(m \frac{y}{R_o} \frac{M_t}{(1-M_{or})} \frac{r}{r_t} \right) \cdot$$

$$\left(\frac{x}{R_o} dF_x + \frac{1-M_{or}}{M_t} \frac{r_t}{r} dF_\theta \right) .$$

5. Extension to B Blades

For an assembly of B identical blades, the usual phase arguments show that only harmonics which are multiples of B survive, and all the rest cancel Hence only harmonics of the propeller blade passing frequency, $B\omega$ are present in the acoustic field of the complete propeller, and the magnitude of the m^{th} harmonic is BC_{mB}:

$$C_m = \frac{i m B^2 \omega e^{i m \omega \frac{R_o}{a_o}}}{2 \pi a_o R_o (1 - M_{or})} (-i)^{mB} \int J_{mB} \left(mB \frac{y}{R_o} \frac{M_t}{1-M_{or}} \frac{r}{r_t} \right) \cdot$$

$$\left(-\frac{x}{R_o} dF_x - \frac{1-M_{or}}{M_t} \frac{r_t}{r} dF_\theta \right) .$$

Then, the r m.s pressure is given as

$$P_{rms}^2 = \frac{1}{2} \sum_{m=1}^{\infty} \left| C_m \right|^2$$

The total intensity at $\bar{X}$ is,

$$I = \frac{P_{rms}^2}{\rho_o a_o}$$

BEST SELLERS

FROM NATIONAL TECHNICAL INFORMATION SERVICE

NTIS

An Inexpensive Economical Solar Heating System for Homes
N76-27671/PAT 59 p PC$4 50/MF$3 00

Viking I Early Results
N76-28296/PAT 76 p PC$2 00/MF$3 00

Energy Fact Book 1976, Chapters 1 through 21
ADA-028 284/PAT 432 p PC$11 75/MF$3 00

Security Analysis and Enhancements of Computer Operating Systems
PB-257 087/PAT 70 p PC$4 50/MF $3 00

Evaluation of the Air-to-Air Heat Pump for Residential Space Conditioning
PB-255 652/PAT 293 p PC$9 25/MF$3 00

Monitoring Groundwater Quality Monitoring Methodology
PB-256 068/PAT 169 p PC$6 75/MF$3 00

An Air Force Guide to Software Documentation Requirements
ADA-027 051/PAT 178 p PC$7 50/MF$3 00

The Production of Oil from Intermountain West Tar Sands Deposits
PB-256 516/PAT' 98 p PC$5 00/MF$3 00

Analysis of Large Scale Non-Coal Underground Mining Methods
PB-234 555/PAT 581 p PC$13 75/MF$3 00

Who's Who in the Interagency Energy/Environment R and D Program
PB-256 977/PAT 35 p PC$4 00/MF$3 00

Local Area Personal Income, 1969-1974 Volume 2 Central and Northeastern States
PB-254 056/PAT 578 p PC$13 75/MF$3 00

Feasibility of Considerably Expanded Use of Western Coal by Midwestern and Eastern Utilities in the Period 1978 and Beyond
PB-256 048/PAT 61 p PC$4 50/MF$3 00

Availability of Potential Coal Supply Through 1985 by Quality Characteristics
PB-256 680/PAT 121 p PC$5 50/MF$3 00

Flat-Plate Solar Collector Handbook A Survey of Principles, Technical Data and Evaluation Results
UCID-17086/PAT 96 p PC$5 00/MF$3 00

HOW TO ORDER

When you indicate the method of payment, please note if a purchase order is not accompanied by payment, you will be billed an additional $5 00 *ship and bill* charge And please include the card expiration date when using American Express

Normal delivery time takes three to five weeks It is vital that you order by number or your order will be manually filled, insuring a delay You can opt for *airmail delivery* for $2 00 North American continent, $3 00 outside North American continent charge per item Just check the *Airmail Service* box If you're really pressed for time, call the NTIS Rush Handling Service (703) 557-4700 For a $10 00 charge per item, your order will be airmailed within 48 hours Or, you can pick up your order in the Washington Information Center & Bookstore or at our Springfield Operations Center within 24 hours for a $6 00 per item charge

You may also place your order by telephone or if you have an NTIS Deposit Account or an American Express card order through TELEX The order desk number is (703) 557-4650 and the TELEX number is 89-9405

Thank you for your interest in NTIS We appreciate your order

METHOD OF PAYMENT

☐ Charge my NTIS deposit account no ____________
☐ Purchase order no ____________
☐ Check enclosed for $____________
☐ Bill me Add $5 00 per order and sign below (Not available outside North American continent)
☐ Charge to my American Express Card account number

Card expiration date____________
Signature____________
☐ Airmail Services requested

NAME____________
ADDRESS____________
CITY STATE ZIP____________

Item Number	Quantity Paper Copy (PC)	Microfiche (MF)	Unit Price*	Total Price
			Sub Total	
			Additional Charge	
			Enter Grand Total	

All prices subject to change The prices above are accurate as of 3/77

Foreign Prices on Request

Clip and mail to

NTIS
National Technical Information Service
U S DEPARTMENT OF COMMERCE
Springfield Va 22161
(703) 557-4650 TELEX 89-9405

and the total thrust is

$$T_t = \int_0^{r_t} \left(r\Omega + V_F \frac{W_i}{V} \right) \rho_0 \Gamma \, dr$$

6. Method of Solution

The problem to be solved can be stated as follows

Find the circulation distribution along the lifting line such that I is minimum and T_t constant.

The solution then proceeds as follows.

Expand Γ as Fourier series with coefficients A_i, then

$$I = I(A_1, A_2, A_3 \cdots) = I(A_i)$$

$$T_t = T_t(A_1, A_2, A_3 \cdots) = T_t(A_i)$$

Let $J = I - b(T_t - T_t(A_i))$

where b is a Lagrangian multiplier.

A necessary condition that I be extremum is

$$\frac{\delta J}{\delta A_i} = 0 \qquad i = 1, 2, 3, \cdots$$

Solve equation (A) and (B) for A_i and b